Nuevas técnicas para el desarrollo de materiales mediante el uso de antimateria
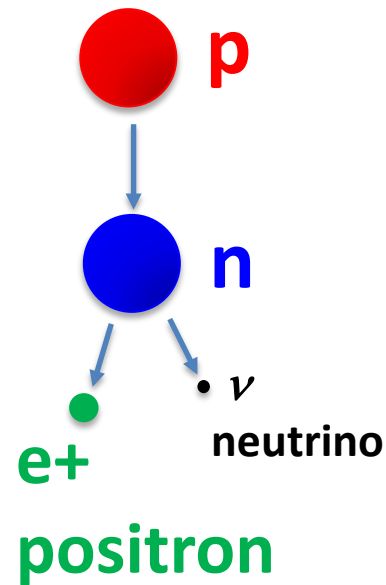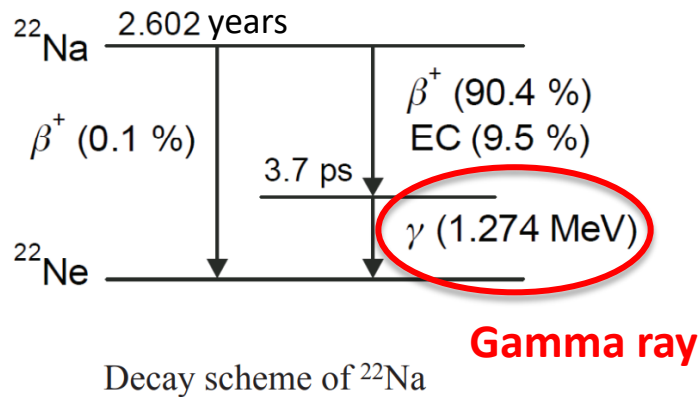
Positron Annihilation Spectroscopy

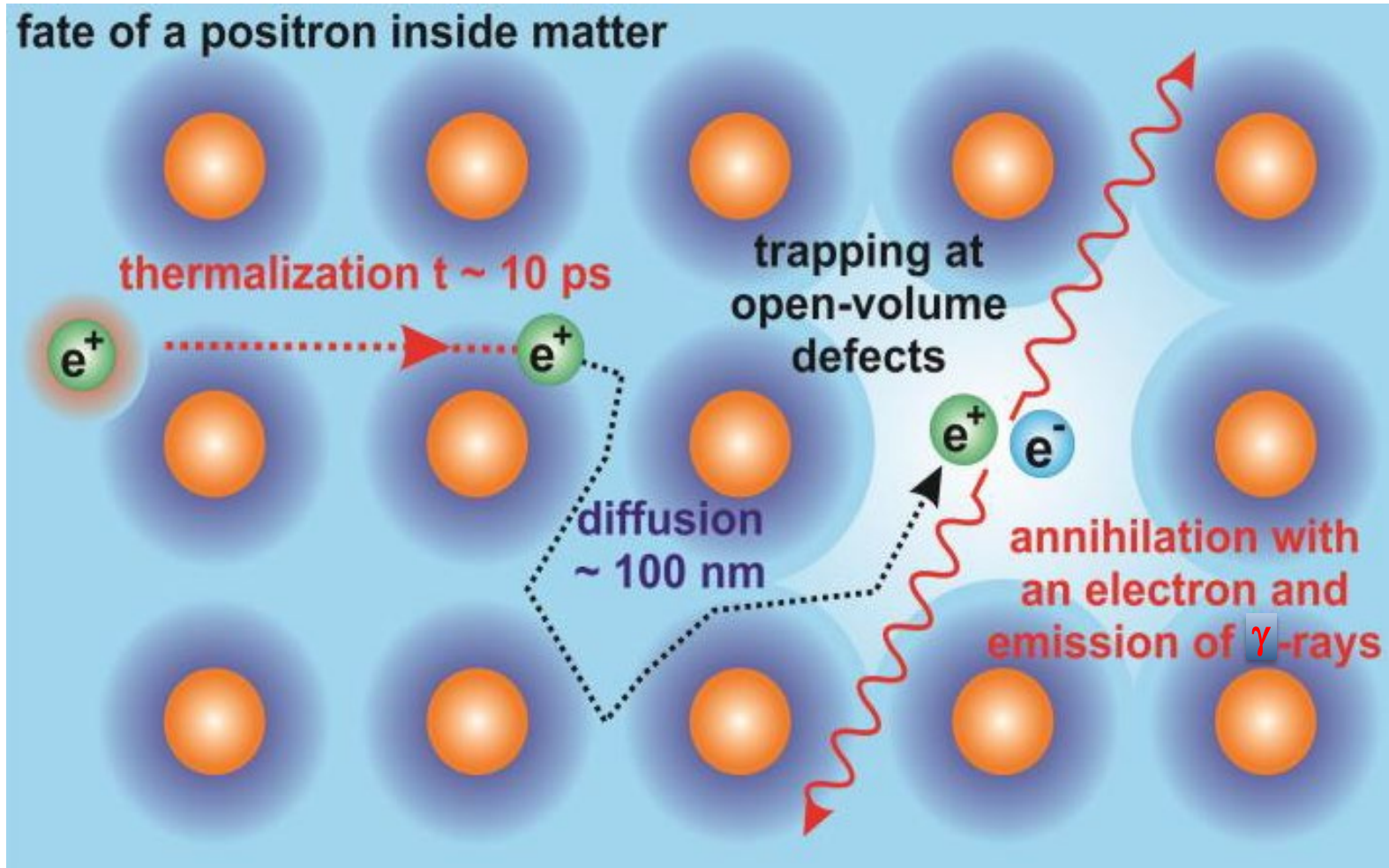**Rafael Ferragut**

²²Na is produced by bombardment of Mg target with suitable projectiles such as protons, deuterons or α particles.

Decay scheme of ²²Na

Gamma ray

p

n

e+
positron

ν
neutrino

- β^+ decay: $^{22}\text{Na} \rightarrow {}^{22}\text{Ne} + \beta^+ + \nu_e + \gamma_{(1.27\text{MeV})}$

- 1.27 MeV γ appears almost simultaneously with positron - can be used as start event for lifetime spectroscopy

Positron inside matter

fate of a positron inside matter

thermalization t ~ 10 ps

trapping at open-volume defects

diffusion ~ 100 nm

annihilation with an electron and emission of γ-rays

After thermalization:

o Classical point of view: following the diffusion theory, the positron diffuses tens to hundreds of nanometers (diffusion length) and then annihilates with an electron of the crystal.

o Quantum mechanics point of view: the positron wave function is expanded inside a defect free crystal before annihilation with an electron wave.

o Possible agreement: the positron diffusion length is of the order of the "radius" of the expansion volume of the wave function.
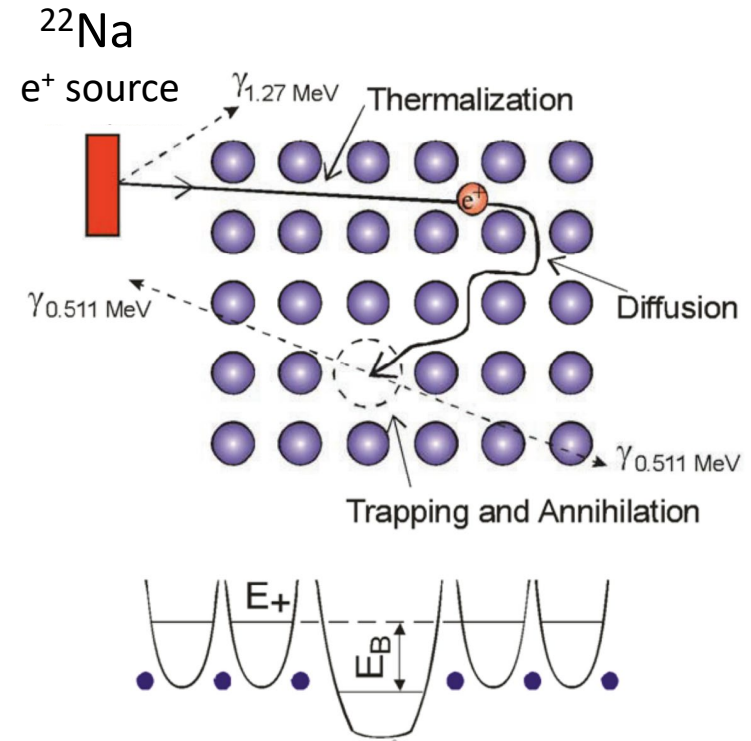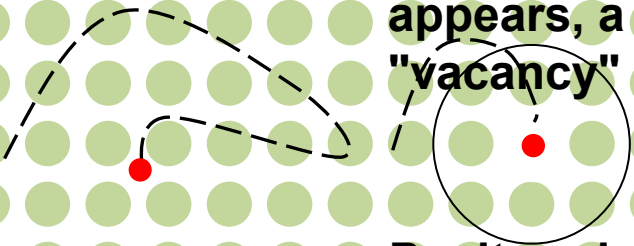
Positron in a crystal
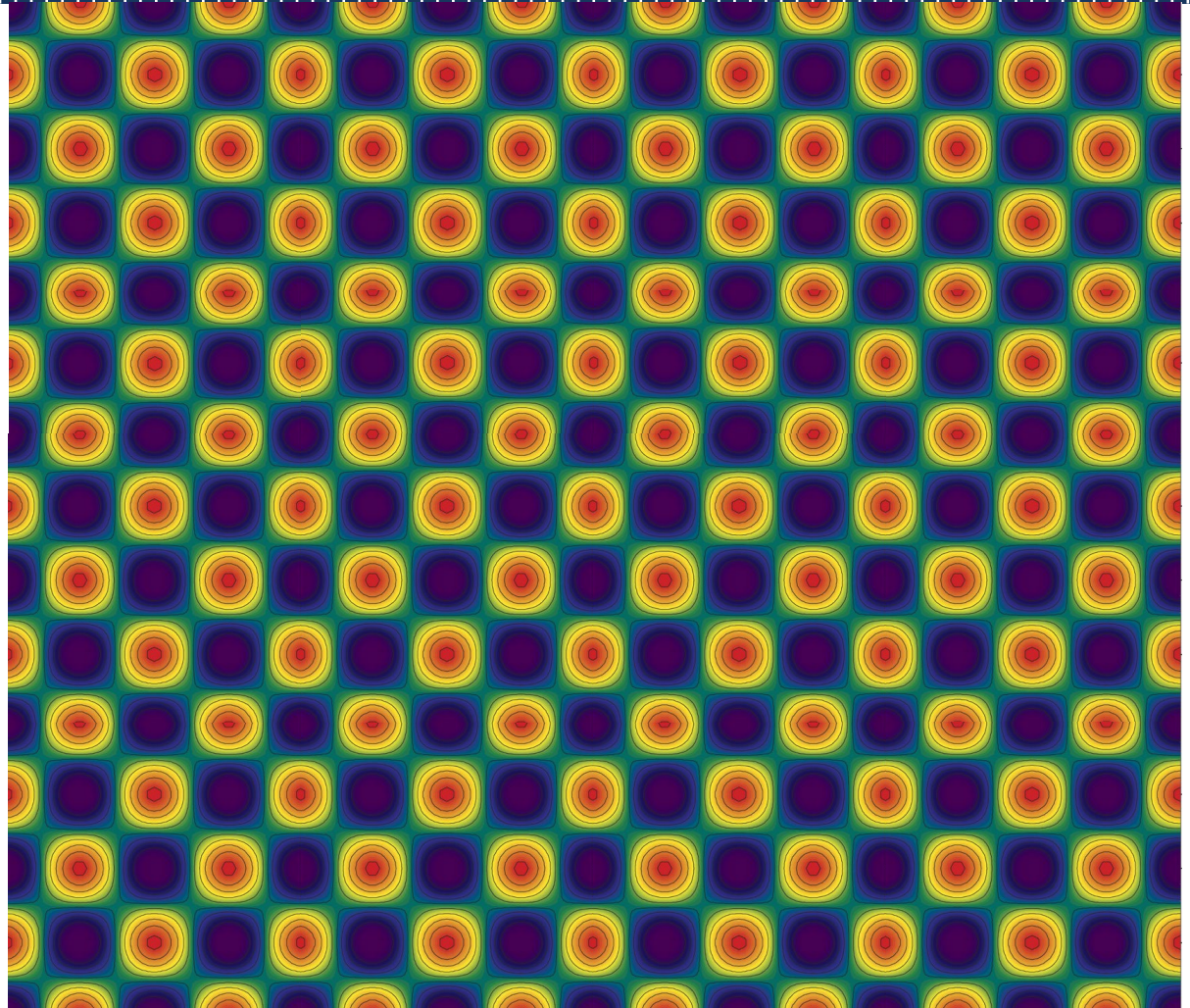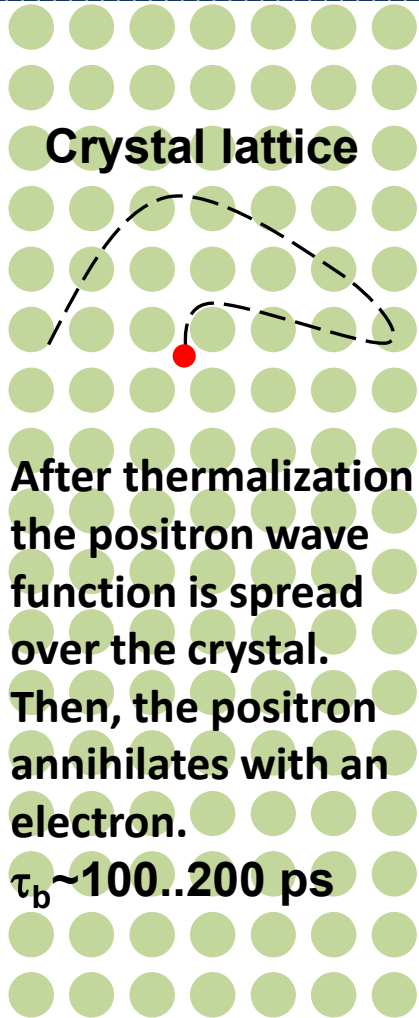
Crystal lattice

After thermalization the positron wave function is spread over the crystal. Then, the positron annihilates with an electron.
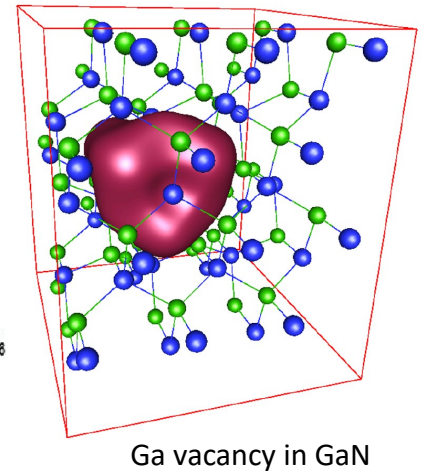$\tau_b \sim 100..200$ ps
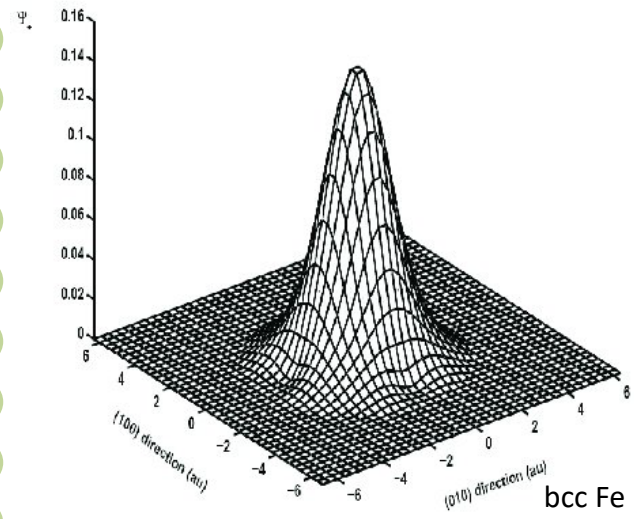
Positron in a crystal

Crystal lattice

An atom is missing. A defect appears, a "vacancy"

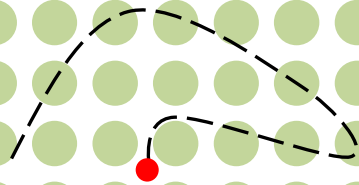**After thermalization the positron diffuses and annihilates with an electron $\tau_b \sim 100..200$ ps**

Positron is trapped and the lifetime is increased, about 50% in Al ($\tau_v > \tau_b$)

bcc Fe

Ga vacancy in GaN

Localized positron wave function in a vacancy; isometric plot.

Positron in a crystal

Crystal lattice

After thermalization the positron diffuses and annihilates with an electron $\tau_b \sim 100..200$ ps

An atom is missing. A defect appears, a "vacancy"

Positron is trapped and the lifetime is increased, about 50% in Al ($\tau_v > \tau_b$)

Contains larger defects «voids»
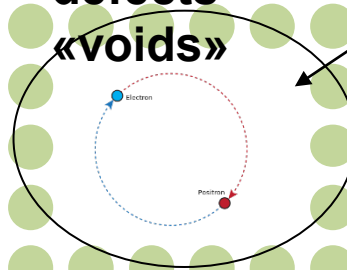
The lightest atom, positronium, is formed, a hybrid (matter/antimatter)
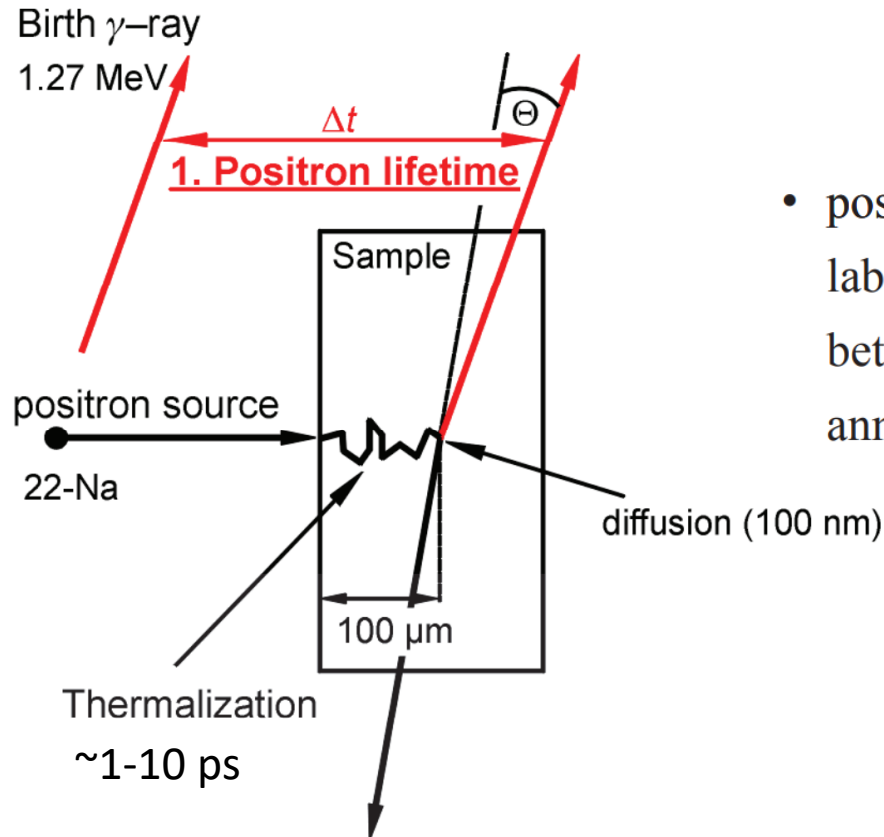
Positronium (Ps) atom
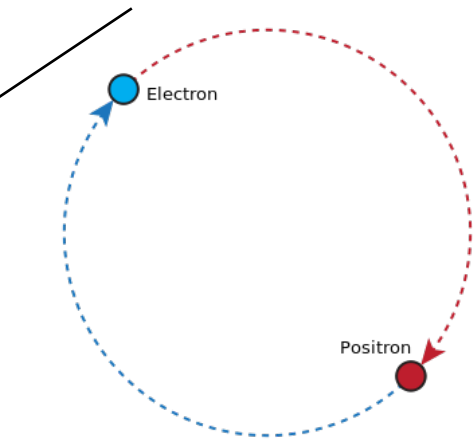
When a positron is bound to an electron its lifetime is increased up to 1000 times !!! ... Ps can annihilate in 3 gamma rays.

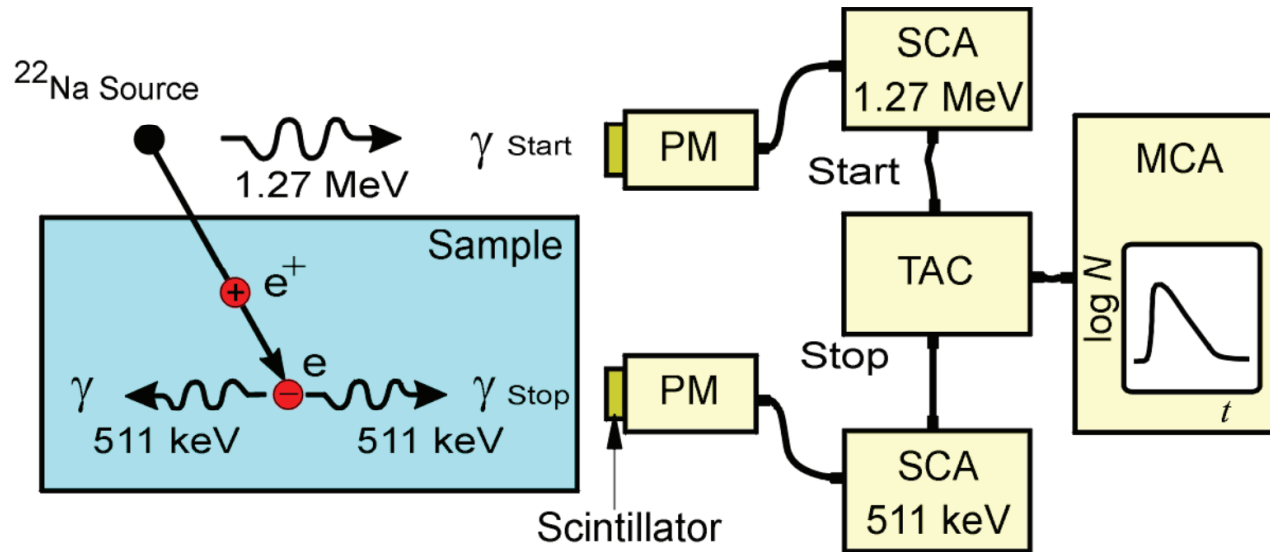# iii. Positron lifetime spectroscopy

- positron lifetime is measured in a ^{22}Na laboratory setup as the time difference between the 1.27 MeV "start" and the annihilation 0.511 MeV "stop" gamma quanta.

The conventional Positron Lifetime Measurement

- Positron lifetime is measured as time difference between 1.27 MeV quantum (β^+ decay) and 0.511 MeV quanta (annihilation process)
- PM…photomultiplier; SCA…single channel analyzer (constant-fraction type); TAC…time to amplitude converter; MCA… multi channel analyzer

Data analysis

The analysis of the spectrum is performed thanks to specific software suites, such as LT software[1].

It is possible to resolve the deconvolution of the resolution function and analyze the components.

$$S(t) = \left(\sum_{i=1}^{n} \frac{I_i}{\tau_i} e^{-\frac{t}{\tau_i}} \right) \star R(t) + B$$

$$\sum_{i=1}^{n} I_i = 1$$

$$\frac{1}{\tau} = \lambda = \pi r_e^2 c \int |\psi_+(\mathbf{r})|^2 n_-(\mathbf{r}) d\mathbf{r}$$
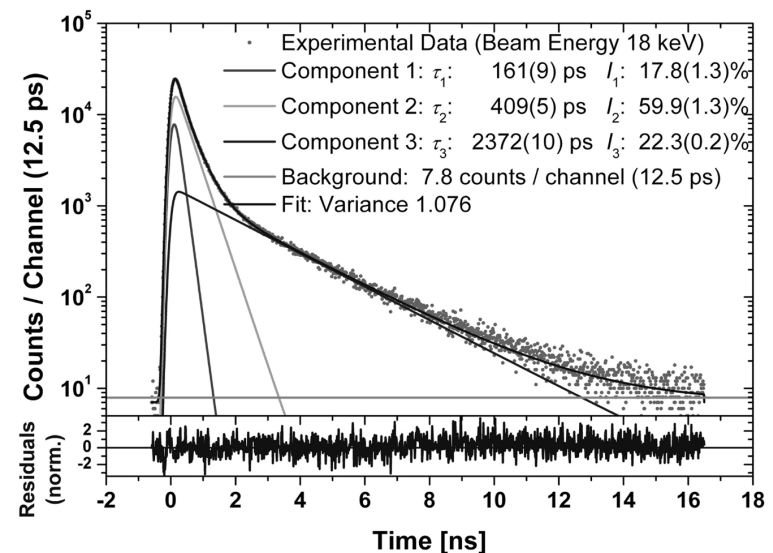
λ: positron annihilation rate
$\psi_+(\mathbf{r})$ is the positron wave function.
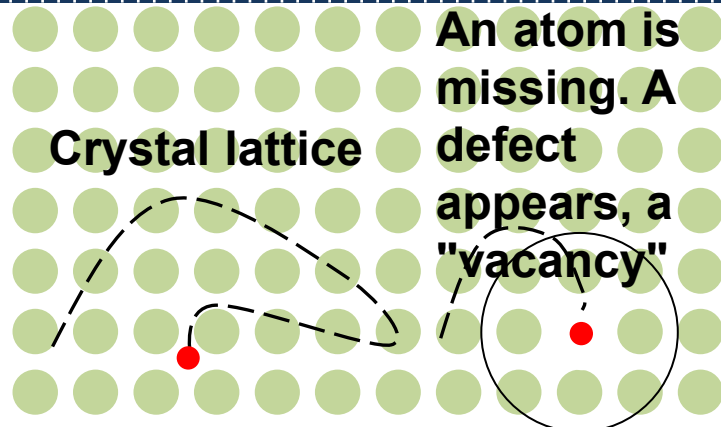$n_-(\mathbf{r})$ is the electron density.

Typical positron lifetime spectrum in an epoxy-based industrial adhesive. The positron implantation energy was 18 keV according to a mean implantation depth of 4 µm. The spectrum can be decomposed into three exponentials with three different lifetimes.

1 J. Kansy, Microcomputer program foranalysis of positron annihilation lifetimespectra. Nucl. Instrum. Methods Phys. A **374**, 235 (1996).

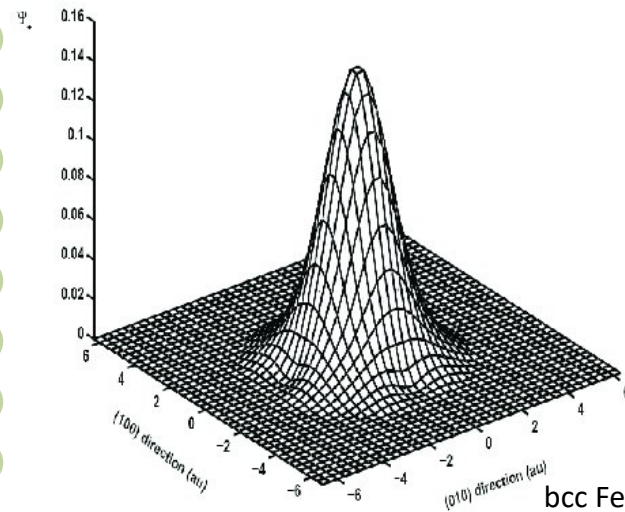# Positron in a crystal

Crystal lattice

An atom is missing. A defect appears, a "vacancy"

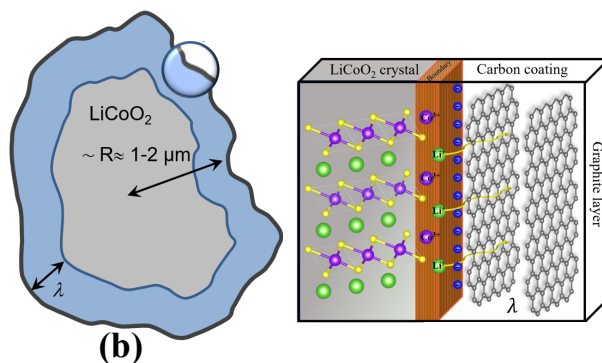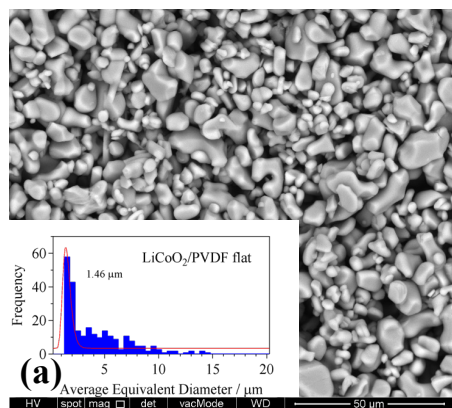**After thermalization the positron diffuses and annihilates with an electron $\tau_b \sim 100..200$ ps**

Positron is trapped and the lifetime is increased, about 50% in Al ($\tau_v > \tau_b$)
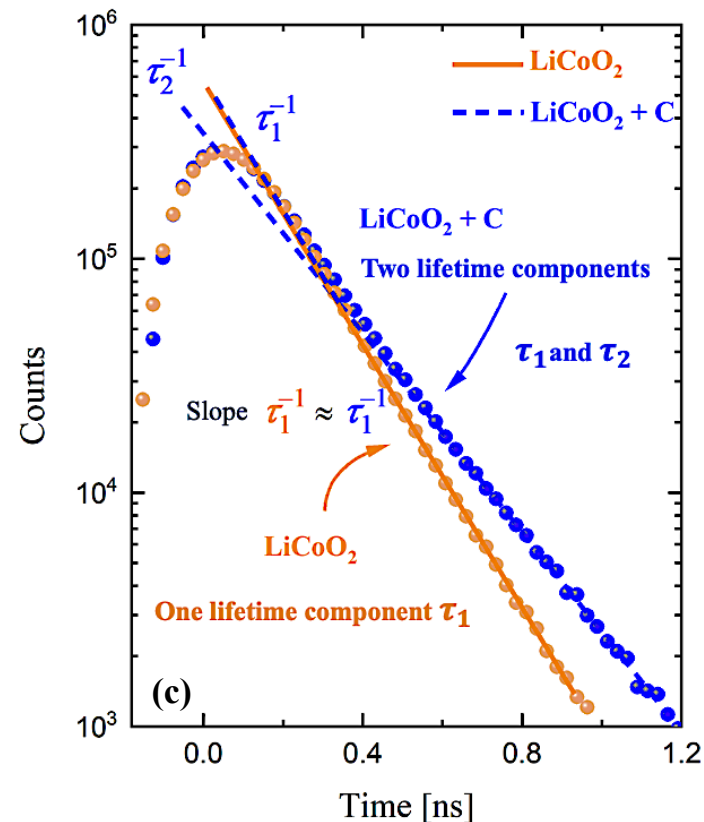

bcc Fe

Localized positron wave function in a vacancy; isometric plot.

LiCoO₂ Samples with Carbon Coating

(a) SEM micrograph of the PVDF/LiCoO₂ grains.

(b) Schematic of graphite/LiCoO₂ heterostructure.

(c) Positron lifetime spectra of LiCoO₂ cathodes with different grain boundaries, with (blue) and without (orange) graphite. The slopes are the inverse of the positron lifetime of each component.

LiCoO$_2$ Samples with Carbon Coating
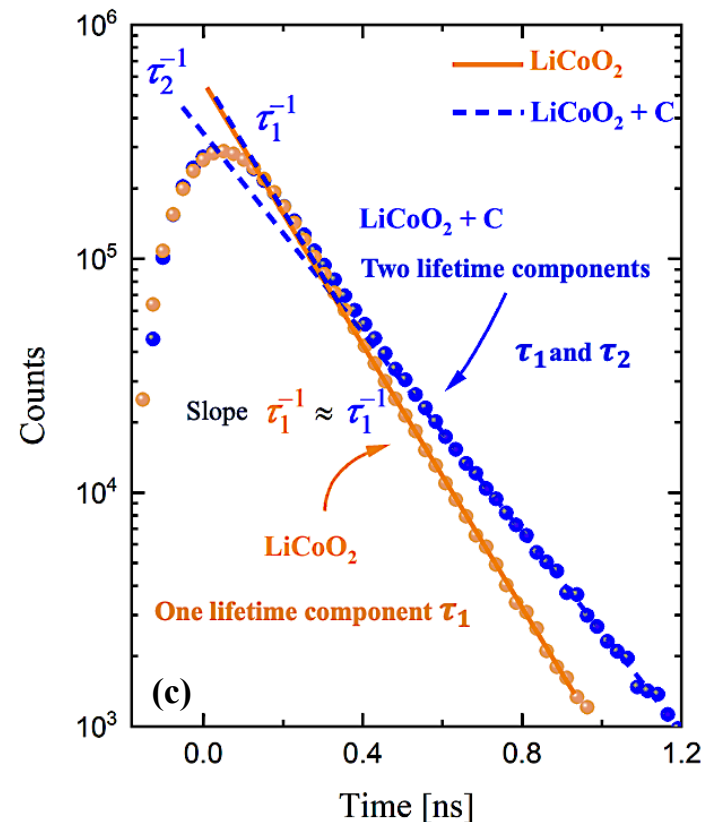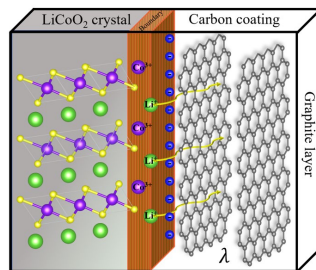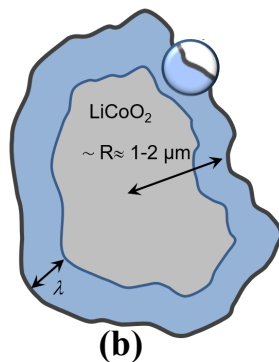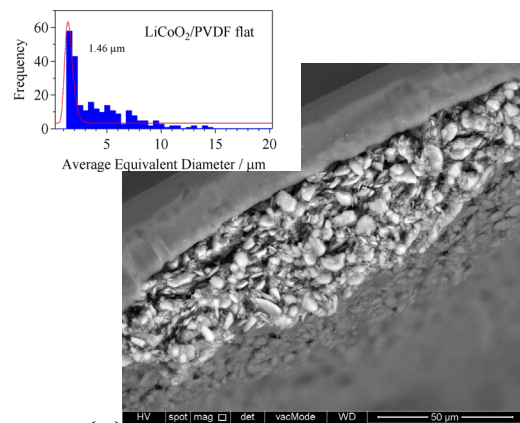
(a) SEM micrograph of the PVDF/LiCoO$_2$ grains.

(b) Schematic of graphite/LiCoO$_2$ heterostructure.

(c) Positron lifetime spectra of LiCoO$_2$ cathodes with different grain boundaries, with (blue) and without (orange) graphite. The slopes are the inverse of the positron lifetime of each component.
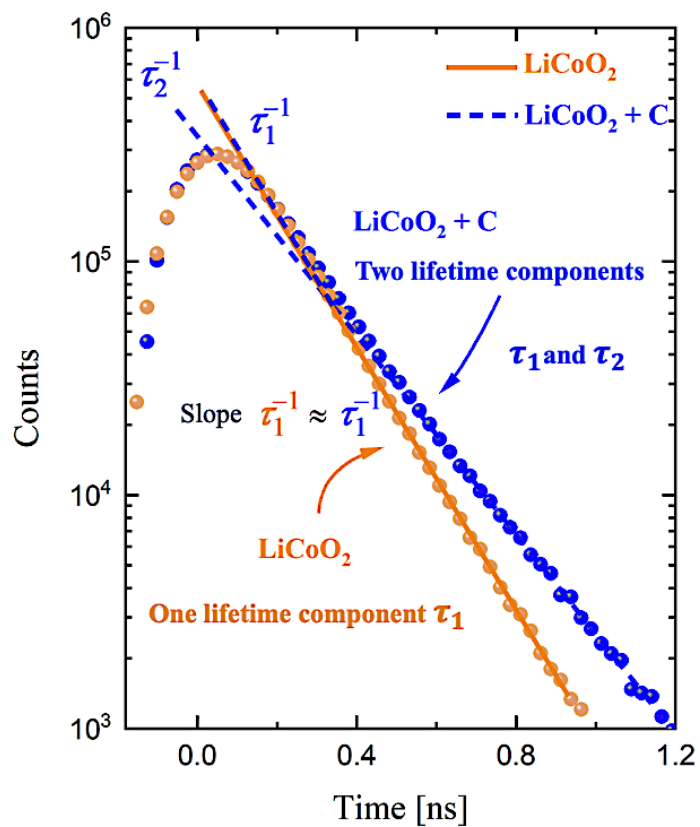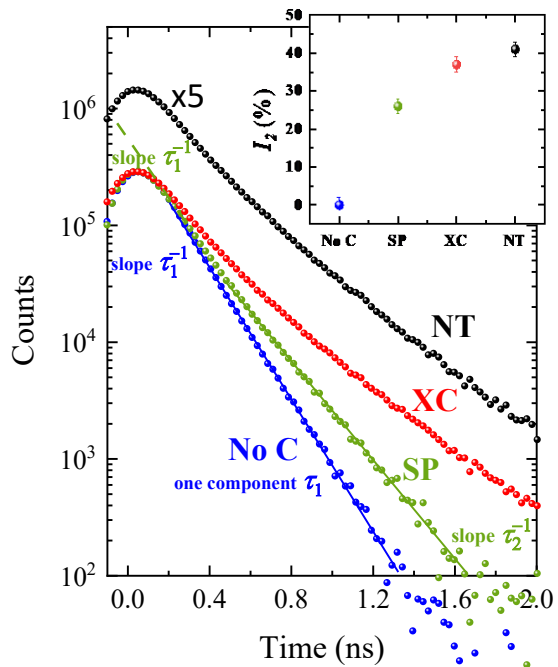
| Cathode		Thickness (μm)	τ_1 (ps)	τ_2 (ps)	I_1 (%)	I_2 (%)	τ (ps)
Exp.	LiCoO2 + PVDF + Graphite	114 (2)	152 (2)	319 (2)	74 (2)	26 (2)	197 (3)
Exp.	LiCoO2 + PVDF	115 (2)	145 (2)	/	100	/	145 (2)
Cal.	LiCoO2 (Perfect Crystal)	/	131	/	/	/	/

Thickness, positron lifetime components, relative intensities and average positron lifetime obtained in the LiCoO2 cathode with and without graphite. Calculated data is based on GGA + LDA.

Positron lifetime spectra of LiCoO$_2$ (LCO) cathodes. Spectra of *SP, XC, NT* and *No C* cathodes.

NoC: without carbon. Only the PVDF   polymer binder
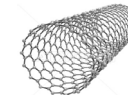
SP: Super P carbon
    Graphite
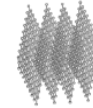
XC: carbon nano-spheres

NT: carbon nano-tubes

G. Pagot, V. Di Noto, K. Vezzù, B. Barbiellini, V. Toso, A. Caruso, M. Zheng, X. Li, R. Ferragut. *Quantum view of Li-ion high mobility at carbon-coated cathode interfaces*. iScience 26, 105794 (2023).
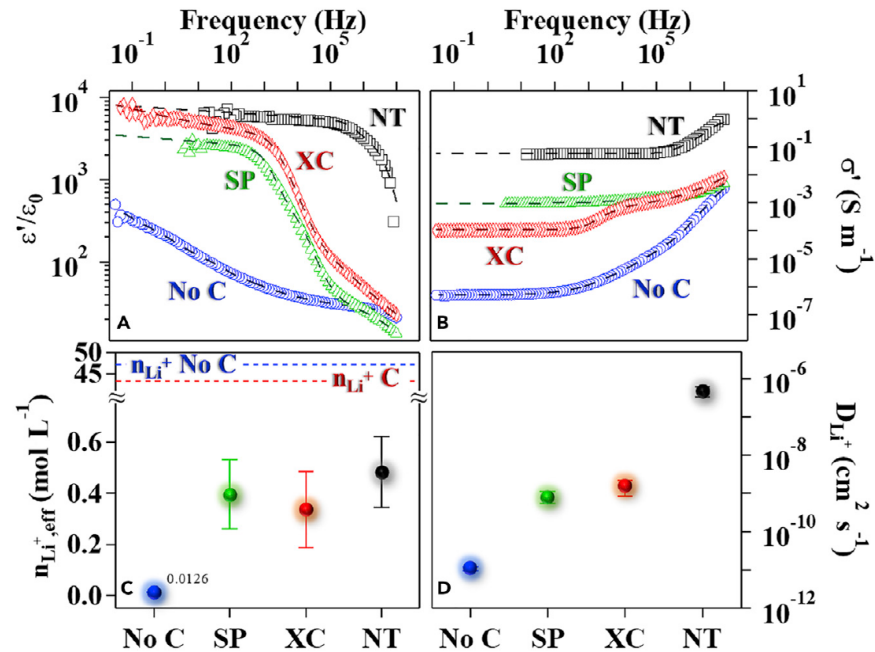
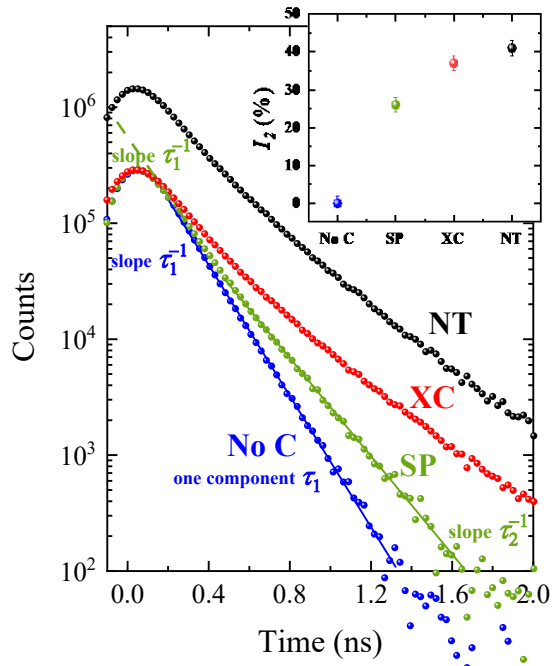**Figure 1. Broadband electrical spectroscopy results**

Real permittivity (ε', A) and conductivity (σ', B) spectra on frequency of the four different samples containing $LiCoO_2$, PVDF and: without carbon (*No C*, blue circles), carbon Super P (*SP*, green triangles), carbon nanospheres (*XC*, red diamonds), and carbon nanotubes (*NT*, black squares). Markers represent experimental data and dashed lines are the fitting results. Concentration of effective mobile lithium ions ($n_{Li^+ eff}$, C) and lithium diffusion coefficient (D_{Li^+}, D) as a function of the carbon employed into the cathode electrode. Error bars (2 *sigma*) are calculated on the basis of the fitting error and experimental data accuracy. Dotted lines in C represent the total lithium ion concentration in the electrodes with (red line) and without (blue line) carbon.
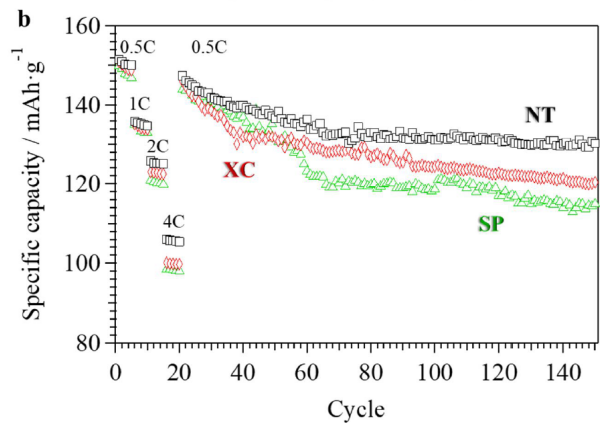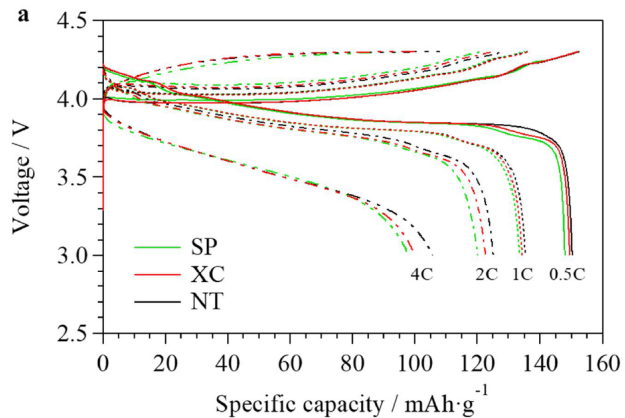
CR2032 battery tests results. Discharge curves are obtained at different current rates (0.5C, 1C, 2C and 4C) with configuration Li | LiPF6 1 M in EC:DMC 1:1 | *cathode*, where *cathode* corresponds to each sample employing SP (green), XC (red) and NT (black) carbon materials (a).

Durability tests in the first 150 cycles at a constant current rate (0.5C) for each sample employing SP (green), XC (red) and NT (black) carbon materials (b).

First-principles calculations
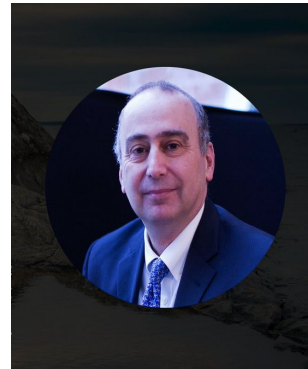

Dr. Ilja Makkonen

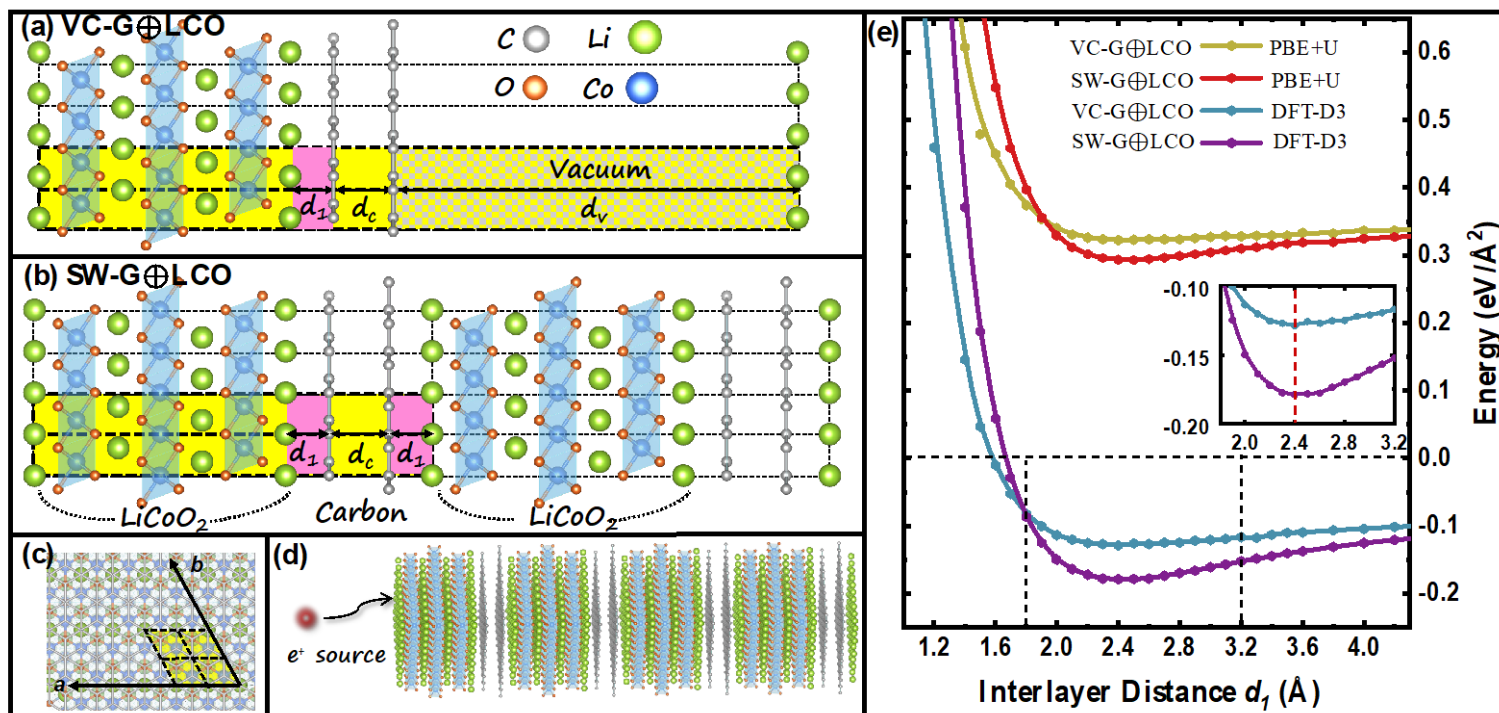UNIVERSITY OF HELSINKI

Dr. Jan Kuriplash
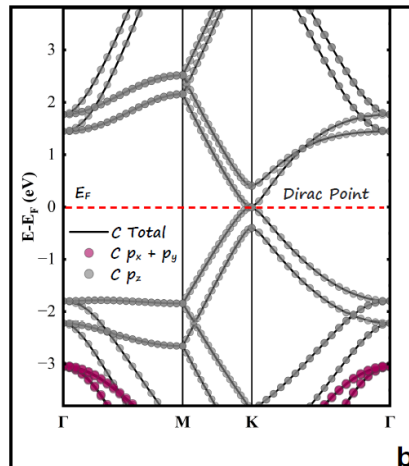
CHARLES UNIVERSITY

Meiying Zheng
PhD student

POLITECNICO MILANO 1863

LUT University

Prof. Bernardo Barbiellini

(a) Vacuum model VC-G⊕LCO **(c)** Top view of SW and VC **(e)** Binding energy of

(b) Sandwich model SW-G⊕LCO **(d)** e$^+$ inject into the SW supercell VC/SW-G⊕LCO heterostructures
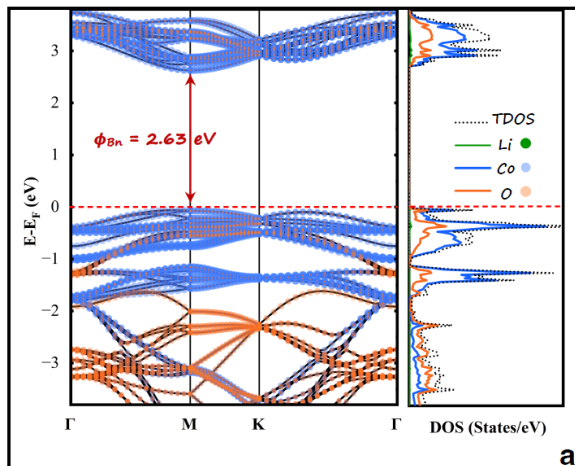
Band structures

(a) Electronic band structure and density of states (DOS) of LiCoO₂ bulk. Total electronic
state, Li, Co, O are shown in black dashed line, lime
green, blue, orange, black solid line, partial band px + py , pz orbitals are shown in purple and gray, respectively. High symmetry line are calculated along Γ, M, K, Γ. Fermi-level is shown in red dashed line.
respectively.
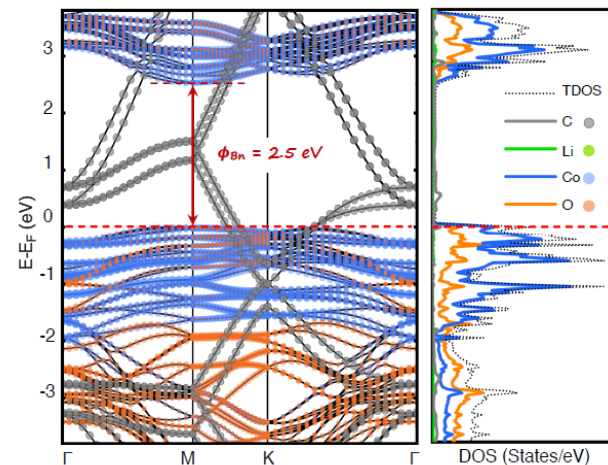
(b) Electronic band structure of free standing graphene layers.

Fig. 2 Electronic band structure and density of states (DOS) of SW-G⊕LCO at the equilibrium distance $d_1 = 2.4$ Å. Total electronic state, C, Li, Co, O are shown in black dashed line, gray, lime green, blue and orange, respectively. High symmetry line are calculated along Γ, M, K, Γ. Dirac point of graphene is located at the K-point and shifts downward by 1.0 eV with respect to the Fermi level shown in red dashed line.

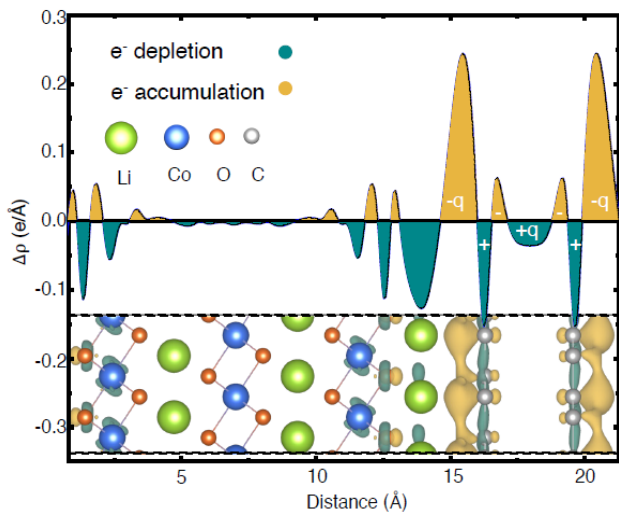# Schematic Diagram of Schottky Barrier
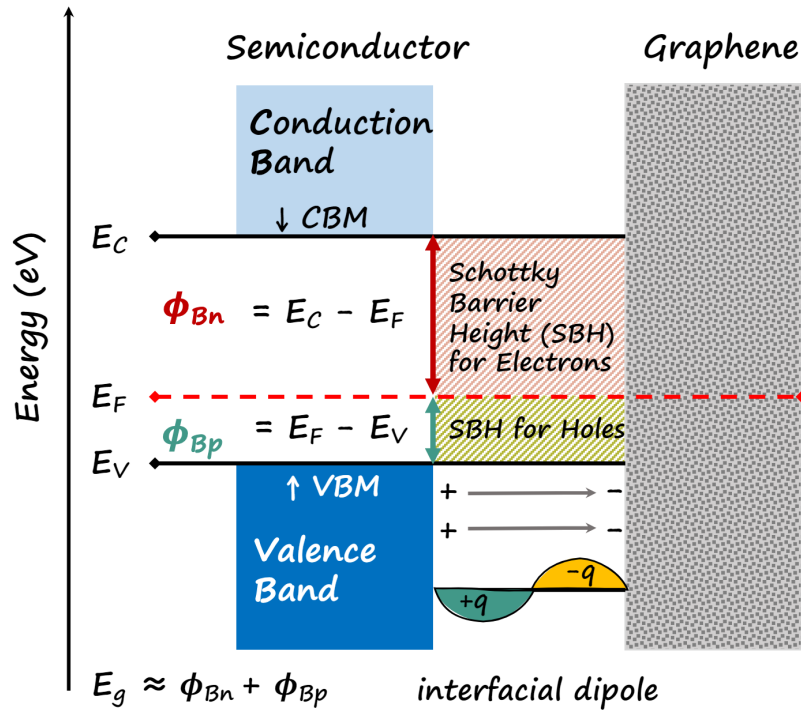
(a) Schematic diagram of Schottky Barrier
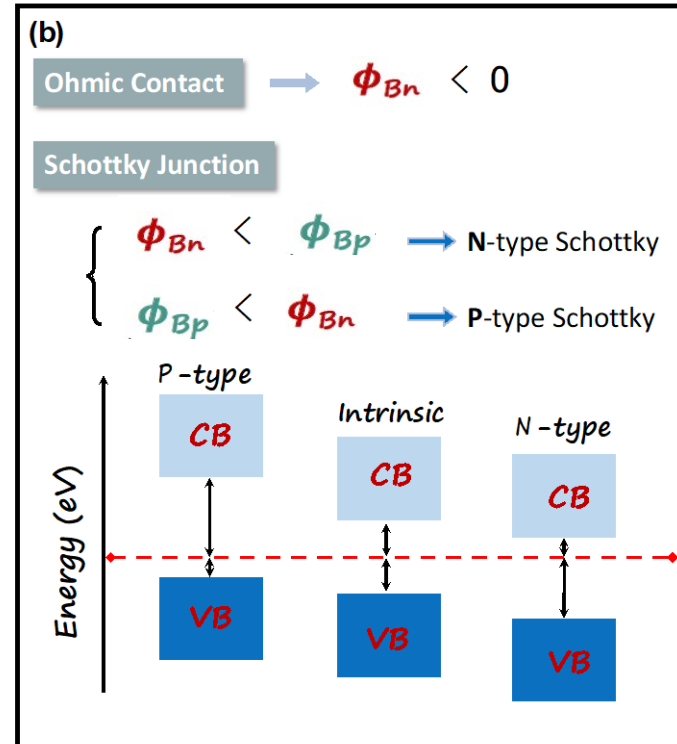
(b) Different interaction types and fermi level position within the band gap for different types of semiconductors.

Positron Annihilation Calculations

Calculated plane-averaged charge density difference of SW-G⊕LCO perpendicular to (001) plane at the equilibrium distance. The corresponding isosurface of charge density difference is the inset. Orange (green) region represents charge accumulation (depletion).
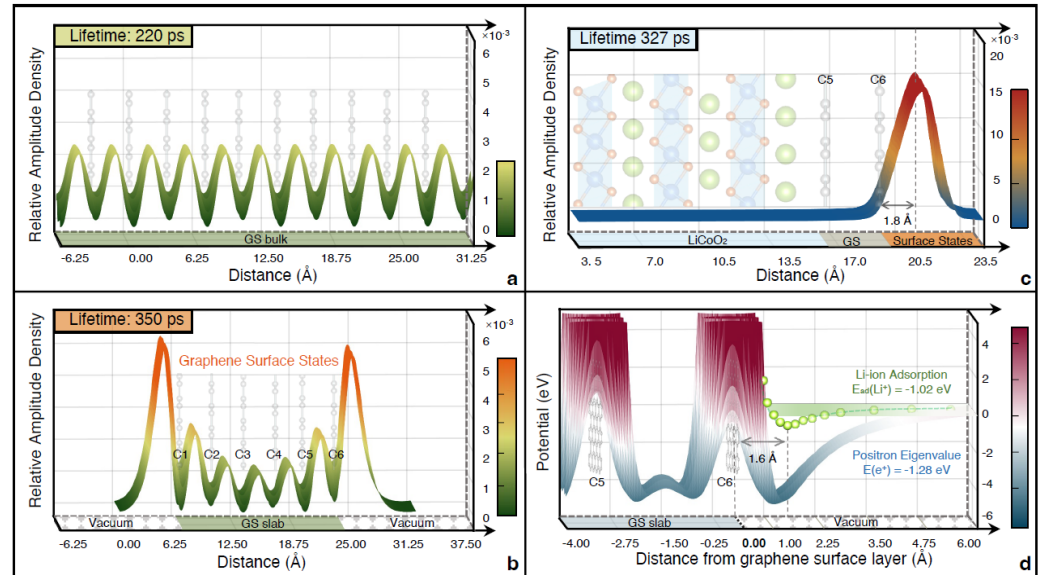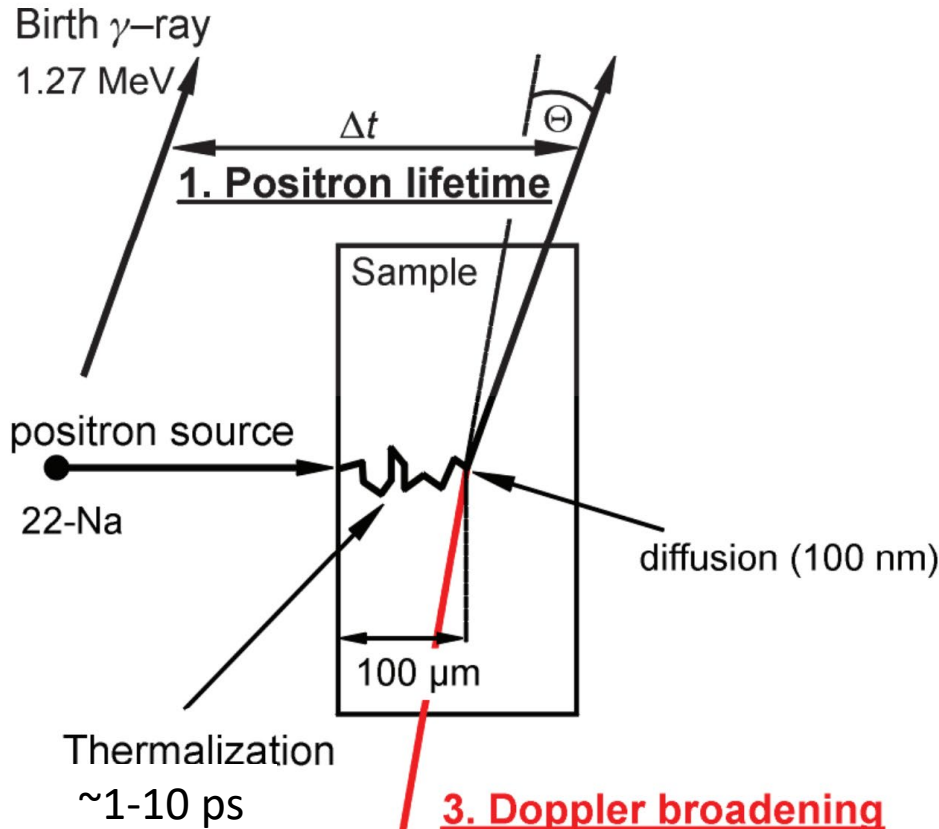

Results of the positron calculations: (a) graphene stack (GS) bulk, (b) six-layer GS slab and (c) SW-G⊕LCO heterostructure. The maximum positron probability density occurs at 1.8 Å from the graphene surface. Ground-state positron densities are presented along c direction. (d) Threedimensional plot of calculated WDA positron total potential in a GS slab.
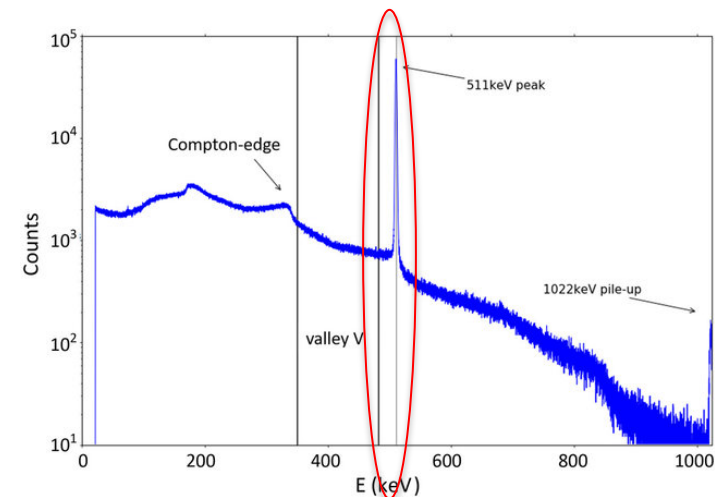
iv. Doppler broadening of the annihilation radiation

Birth γ–ray
1.27 MeV

Δt

1. Positron lifetime

Θ

Sample

positron source

22-Na

diffusion (100 nm)
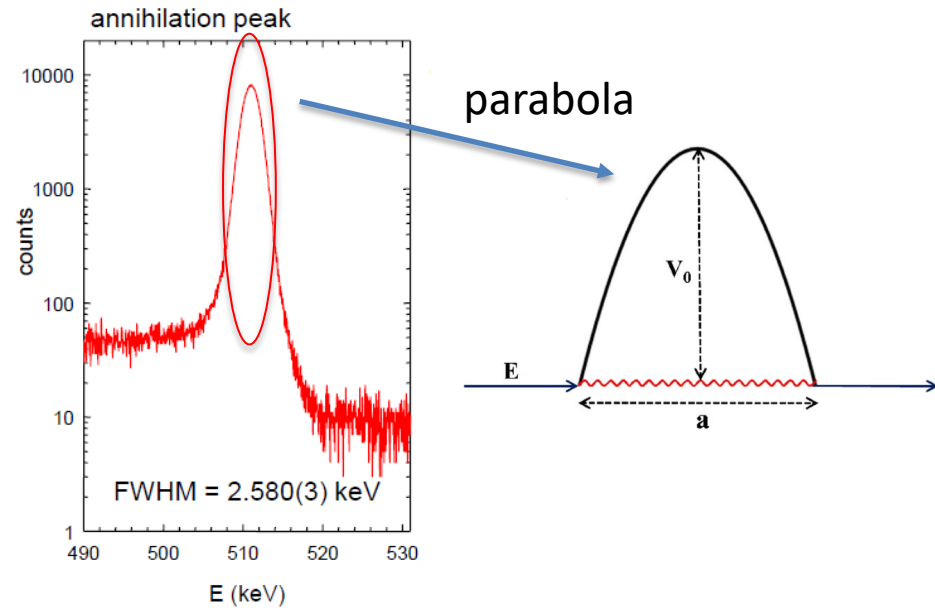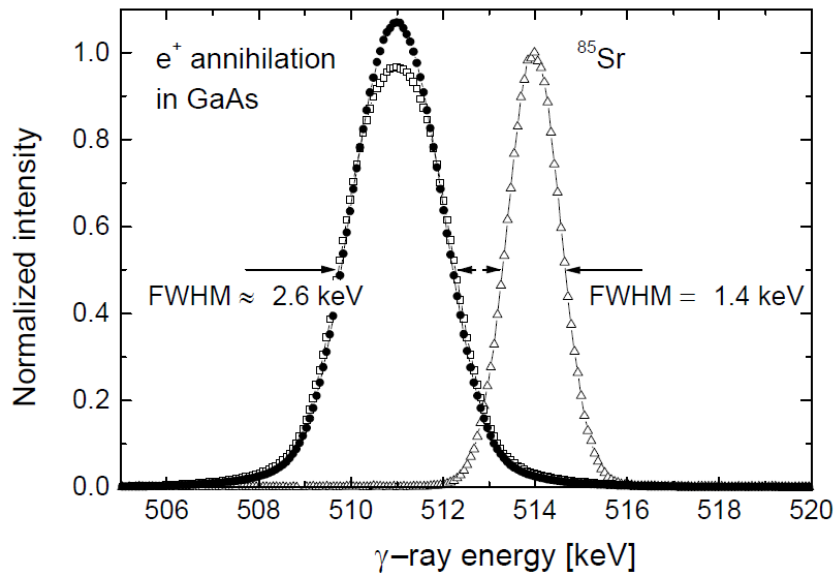
100 µm

Thermalization
~1-10 ps

3. Doppler broadening

0.511 MeV ± ΔE, $\Delta E = p_z c/2 = p_L c/2$

p_L follows the longitudinal direction along the sample and the detector axis

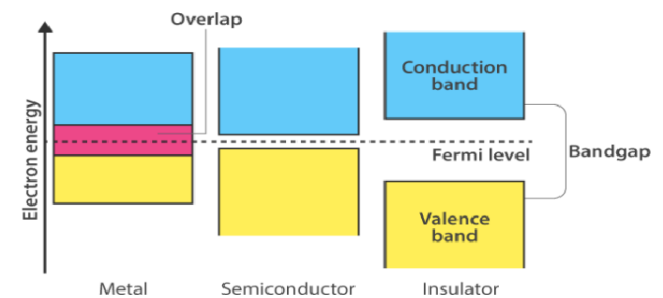Energy spectrum (GeHP)

511keV peak

Compton-edge

1022keV pile-up

valley V

Counts

E (keV)

Doppler broadening Spectroscopy

parabola

The Doppler lines of GaAs are broadened compared with the reference line of ^{85}Sr at 514 keV.
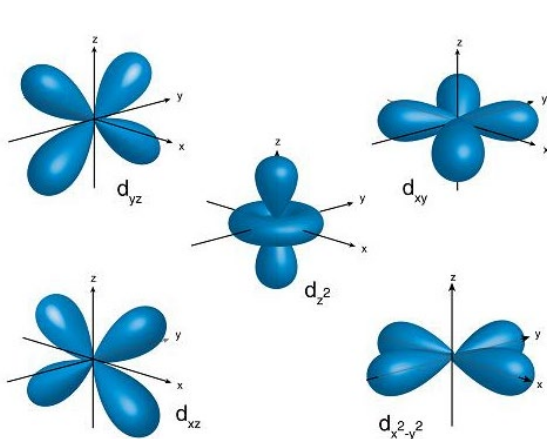
Fitted and experimental Doppler broadening profile spectrum for Fe, including the 3p, 3s and conduction electrons.
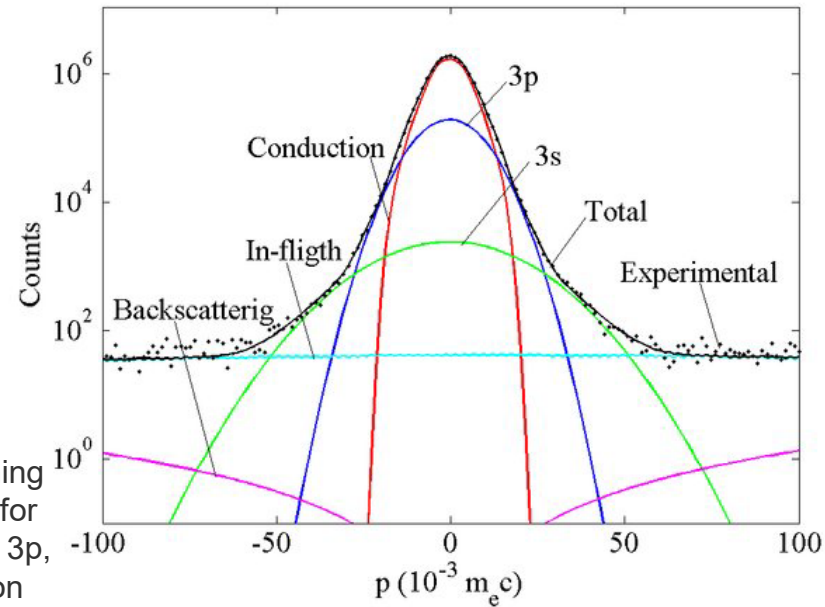
Momentum distribution of the positron-electron pair before annihilation $\rho(\mathbf{p})$

$$\rho(\mathbf{p}) = \pi r_e^2 c \sum_i \left| \int d\mathbf{r}\, e^{-i\mathbf{p}\cdot\mathbf{r}} \psi_+(\mathbf{r}) \psi_i(\mathbf{r}) \right|^2$$

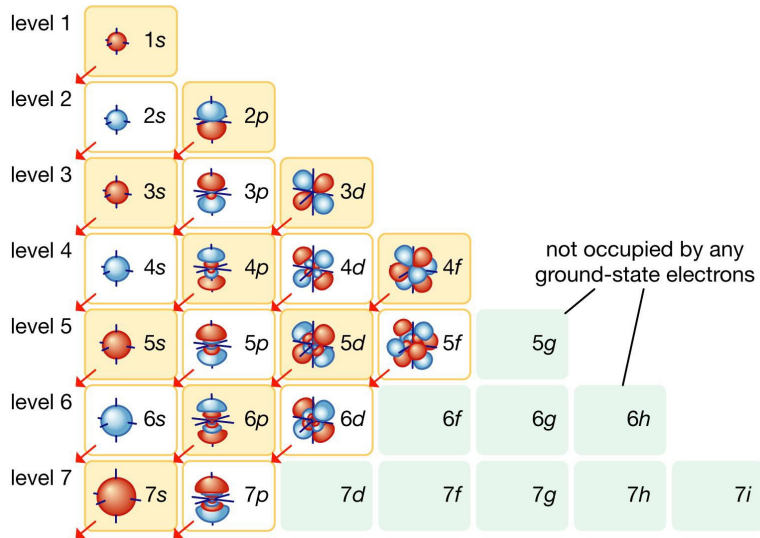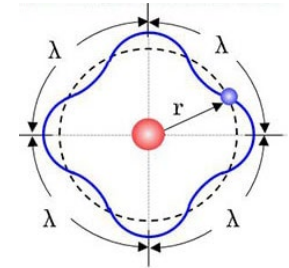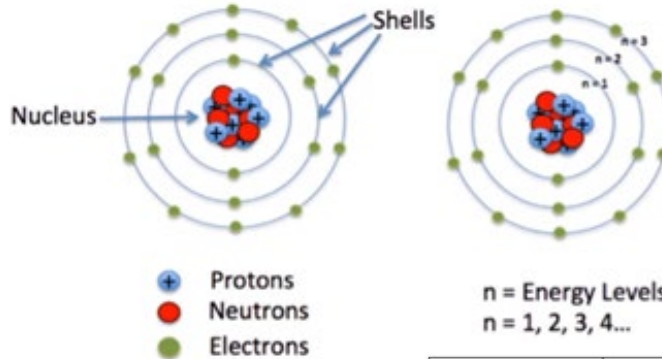$\psi_+(\mathbf{r})$ is the positron wave function.

$\psi_i(\mathbf{r})$ is the electron wave function.

Doppler broadening Spectroscopy
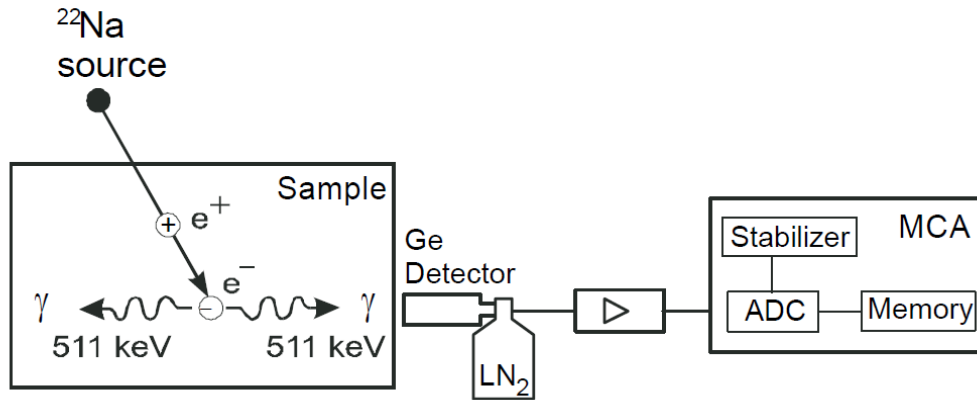
Experimental setup of Doppler-broadening spectroscopy.
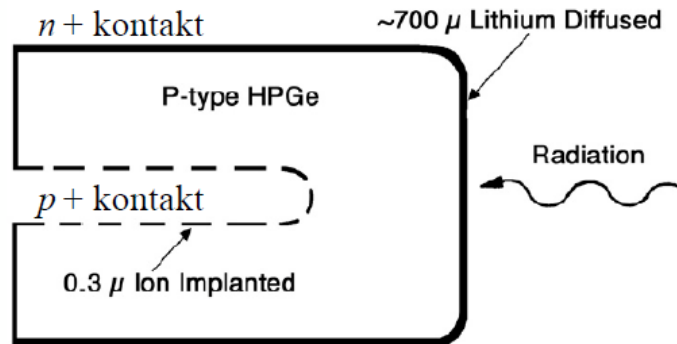
Doppler broadening Spectroscopy

- S parameter

$$S = A_{centr} / A_{tot}$$

|E - 511 keV| < 0.85 keV

Doppler broadening Spectroscopy

- W parameter

$$W = A_{wings} / A_{tot}$$

2.75 keV |E - 511 keV| < 4 keV

POLITECNICO MILANO 1863

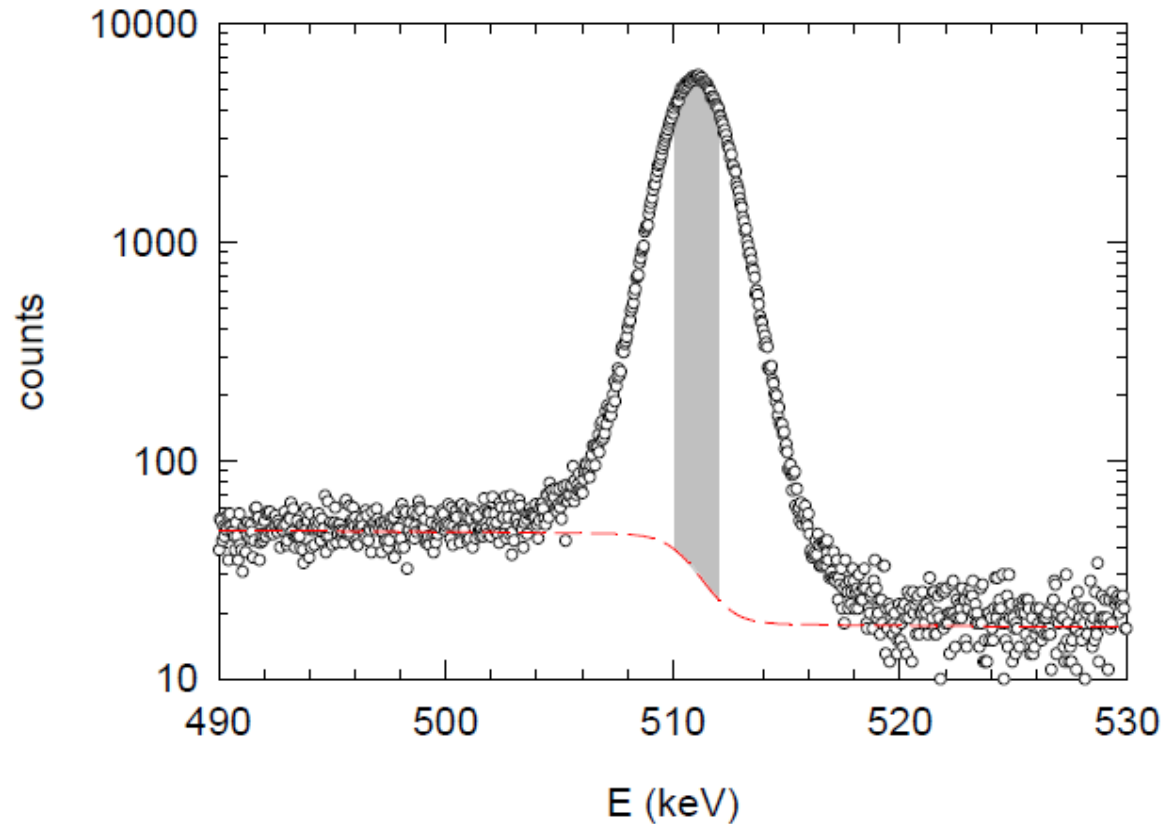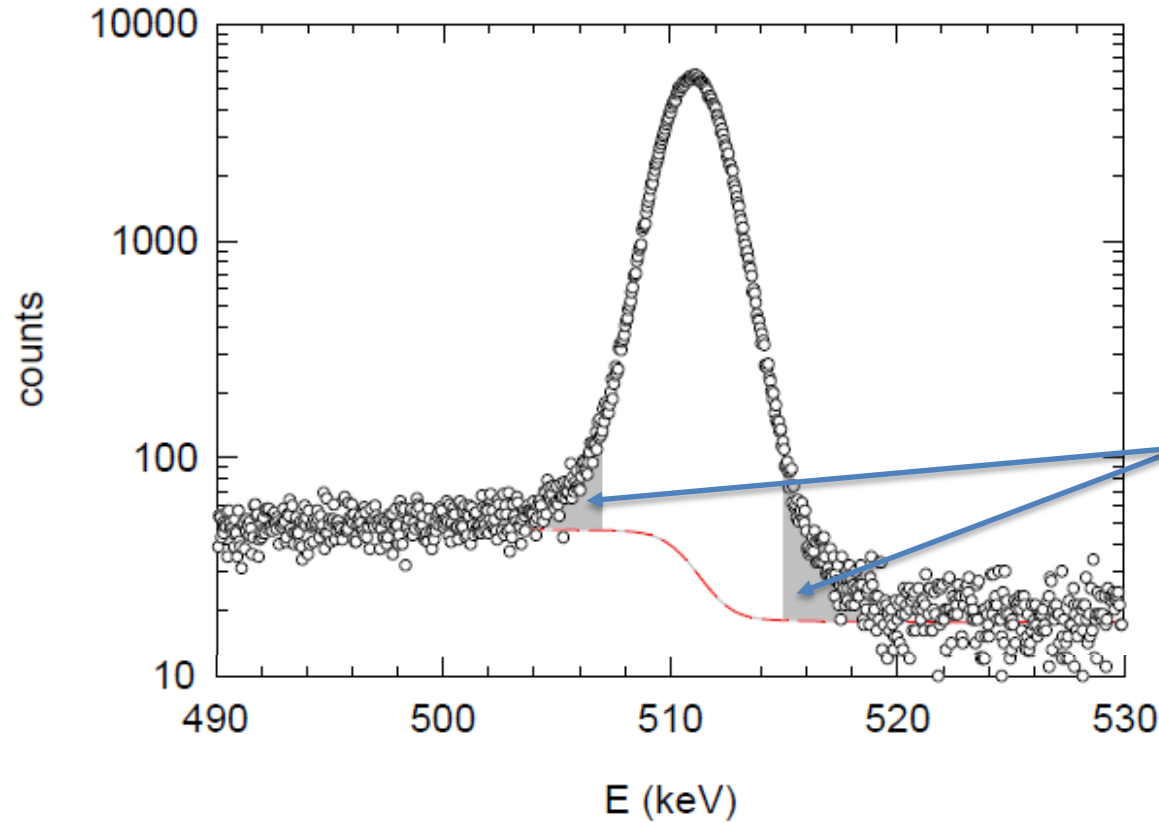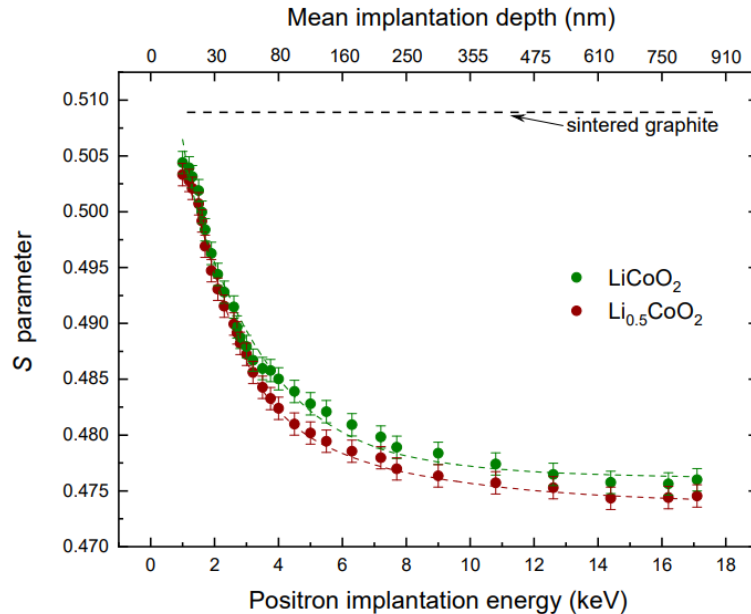**Figure 3.** Evolution of the *S* parameter as a function of the positron implantation energy (mean implantation depth, upper frame) in LiCoO$_2$ (green symbols), in Li$_{0.5}$CoO$_2$ (brown symbols) and in a graphite reference sample (black dashed line). The VEPFIT fitting (green and brown dashed lines) gives an estimation of the positron diffusion length.
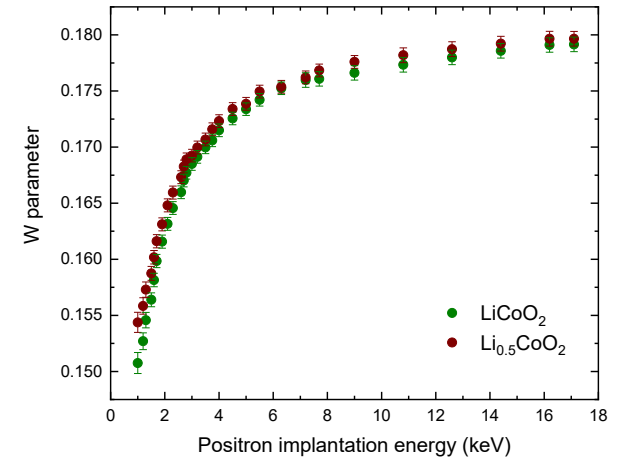
Positron diffusion length
L$_+$≈ 50-60 nm

o J. Nokelainen, B. Barbiellini, J. Kuriplach, S. Eijt, R. Ferragut, X. Li, V. Kothalawala, K. Suzuki, H. Sakurai, H. Hafiz, K. Pussi, F. Keshavarz, A. Bansil. Identifying Redox Orbitals and Defects in Lithium-Ion Cathodes with Compton Scattering and Positron Annihilation Spectroscopies: A Review. Condens. Matter 7 47 (2022).

o G. Pagot, V. Toso, B. Barbiellini, R. Ferragut, V. Di Noto. Positron Annihilation Spectroscopy as a Diagnostic Tool for the Study of LiCoO$_2$ Cathode of Lithium-Ion Batteries. Condens. Matter 6 28 (2021).
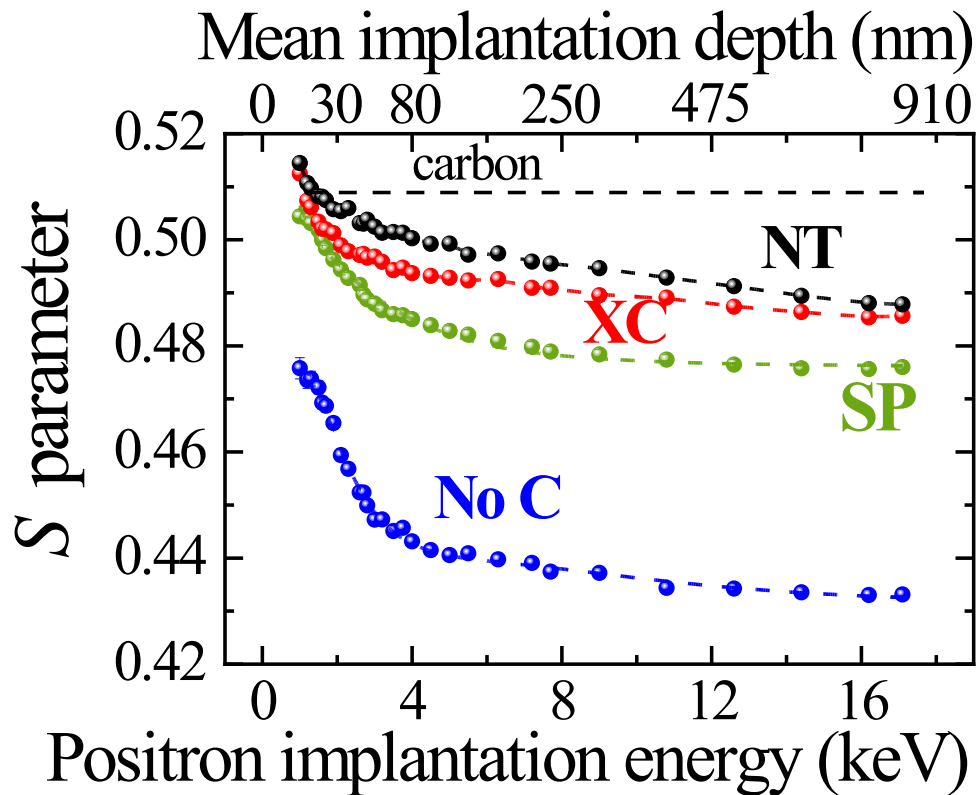
S-parameter LiCoO$_2$ (LCO) cathodes.
Spectra of *SP, XC, NT* and *No C* cathodes.

No C: without carbon. Only the
    PVDF polymer binder
SP: Super P carbon
XC: carbon nano-spheres
NT: carbon nano-tubes

○ G. Pagot, V. Di Noto, K. Vezzu`, B. Barbiellini, V. Toso, A. Caruso, M. Zheng, X. Li, R. Ferragut. *Quantum view of Li-ion high mobility at carbon-coated cathode interfaces*. iScience 26, 105794 (2023).

Defects in GaN films grow by LEPEVPE

GaN film

Sapphire substrate
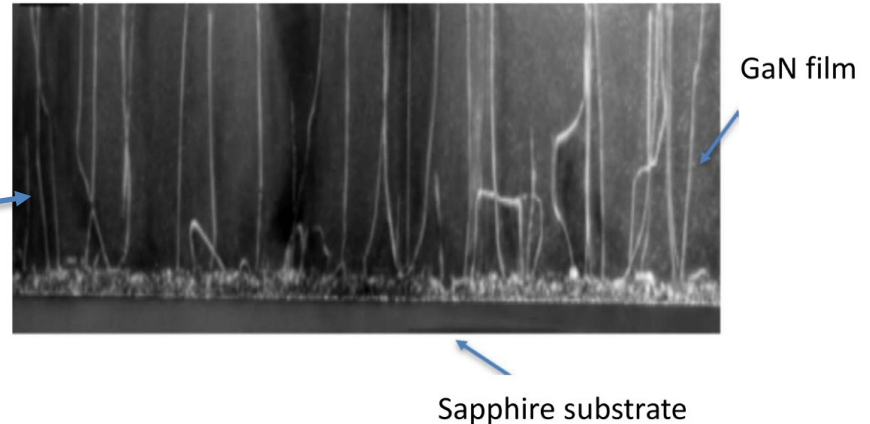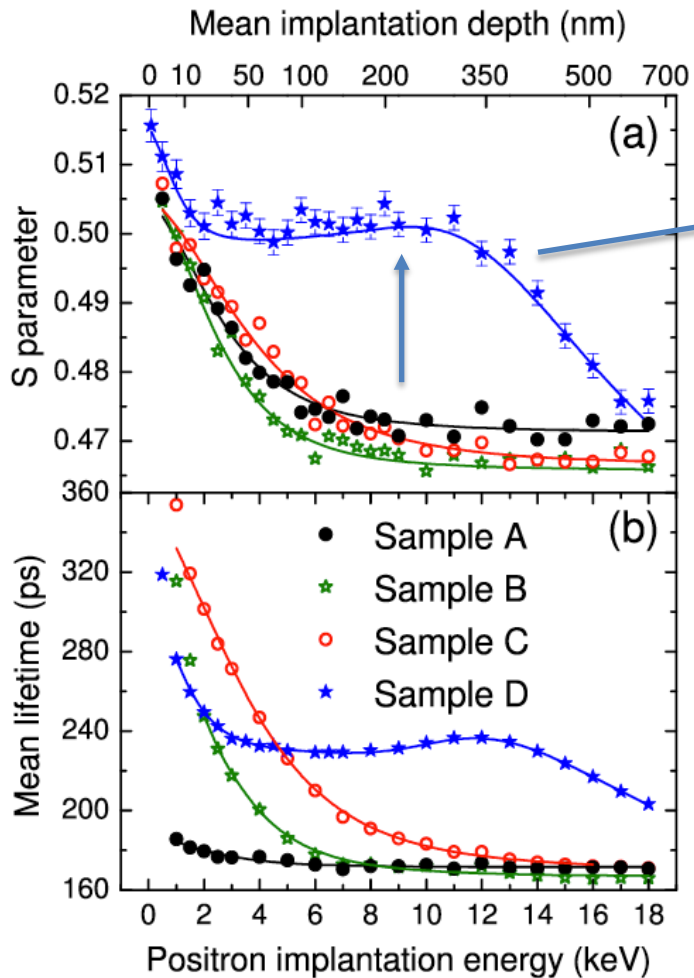
TABLE I. Sample specifications.

Sample	Thickness
A	$3\,\mu m$ GaN/αAl$_2$O$_3$
B	1000 nmGaN[a]/3 μmGaN/αAl$_2$O$_3$
C	1200 nmGaN[a]/3 μmGaN/αAl$_2$O$_3$
D	650 nmGaN[a]/αAl$_2$O$_3$

[a]Grown by LEPEVPE.

LEPEVPE: Low Energy Plasma Enhanced Vapor Phase Epitaxy

A. Calloni, Ferragut, A. Dupaquier, H. von Känel, A. Guiller, A. Rutz, L. Ravelli, and W. Egger: Characterization of vacancy-typedefects in heteroepitaxial GaN grown by Low-Energy Plasma-Enhanced VaporPhase Epitaxy, J. Appl. Phys. 112, 024510 (2012).

Coincidence Doppler Broadening Spectroscopy (CDB)
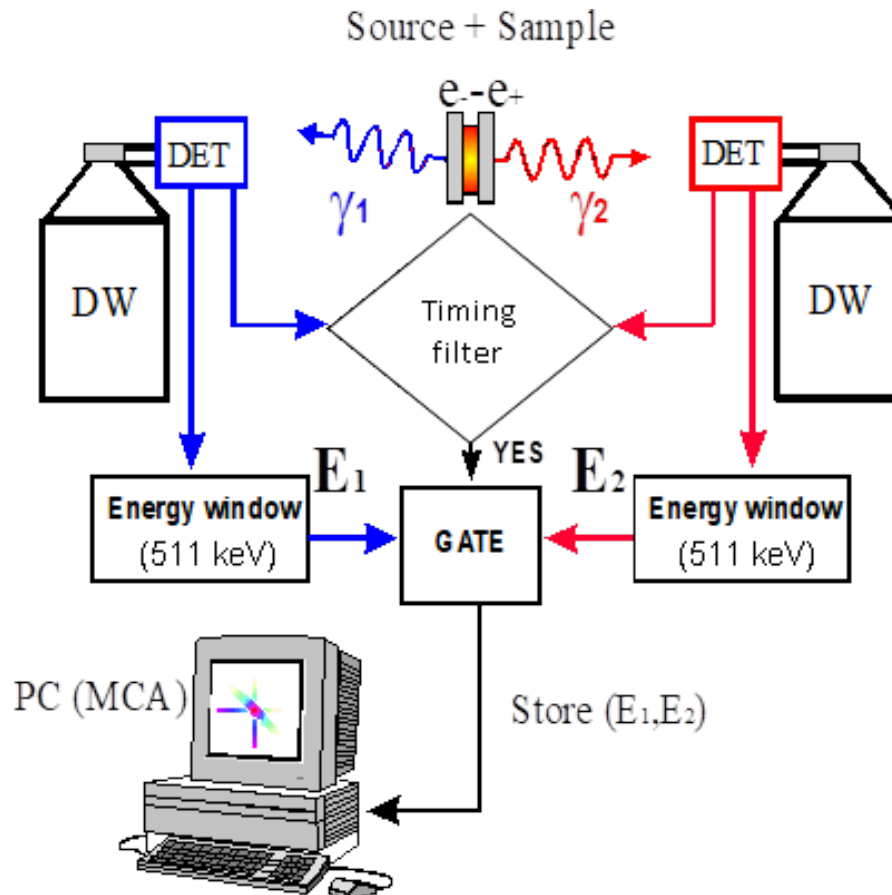
$\Delta E = p_L c/2$ (energy shift)

p_L follows the longitudinal direction along the sample and the detector axes

Coincidence Doppler Broadening Spectroscopy (CDB)
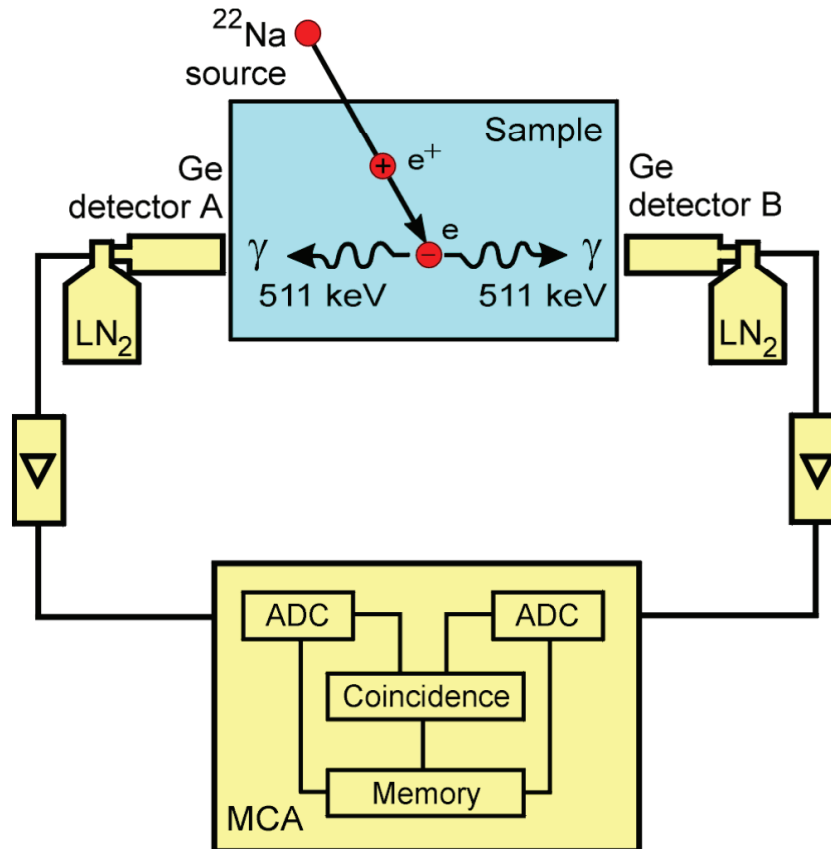
- coincident detection of second annihilation γ reduces background by 3…4 orders of magnitude

- sum of both energies is 1022 keV

- when 515 keV is detected in detector A: detector B shows 507 keV

- thus, electron energy is detected twice

- energy resolution of system is improved by a factor of 0.707

K.G. Lynn et al., Phys. Rev. Lett. 38 (1977) 241; P. Asoka-Kumar et al., Phys. Rev. Lett. 77 (1996) 2097
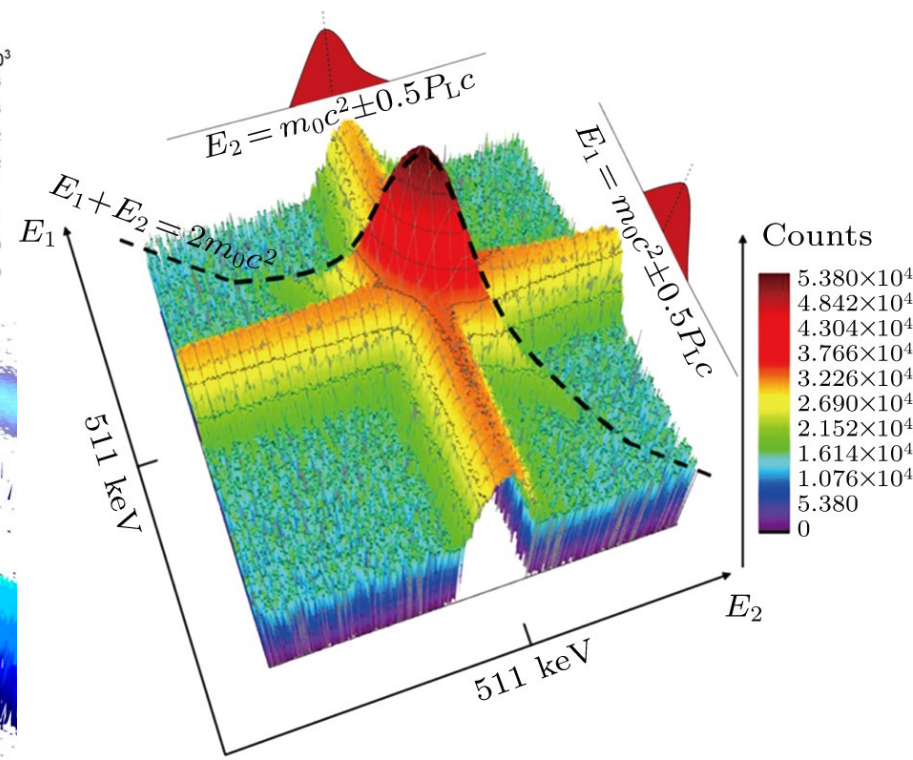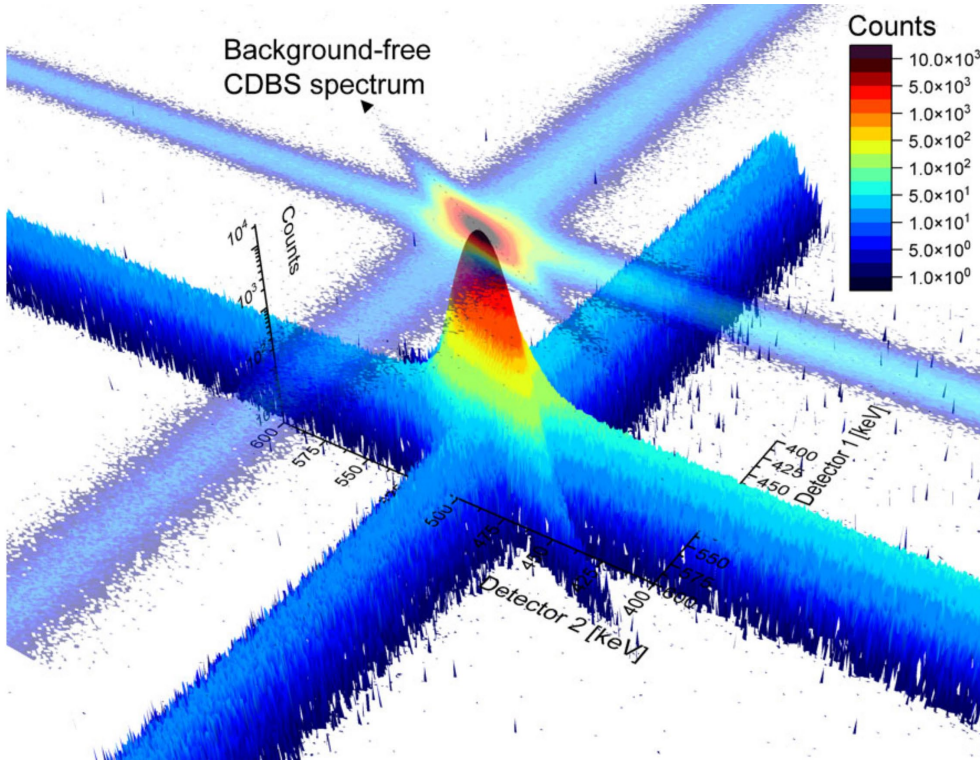
Coincidence Doppler Broadening of the annihilation radiation

$$E_{\gamma 1} + E_{\gamma 2} = 2\, m_0\, c^2 = 1022 \text{ keV}$$
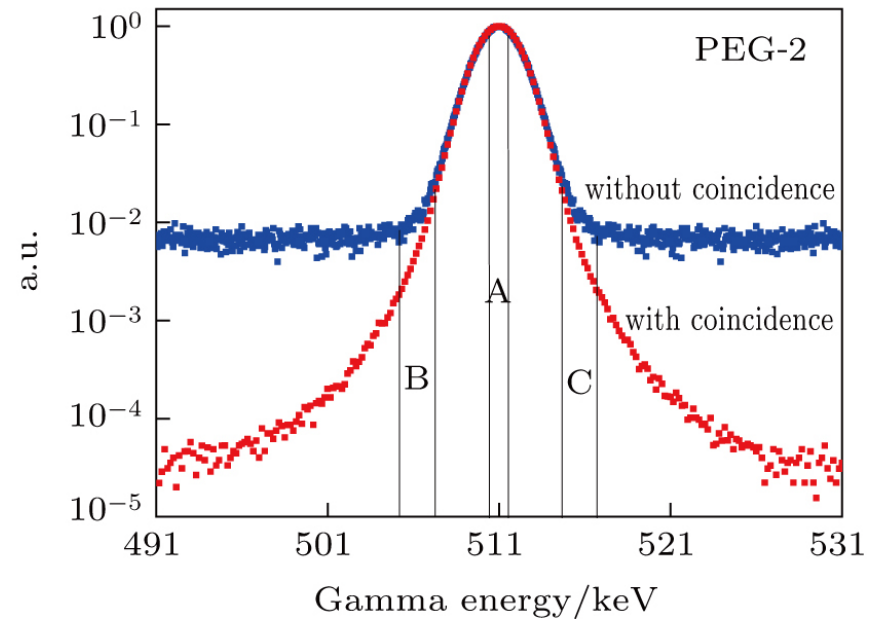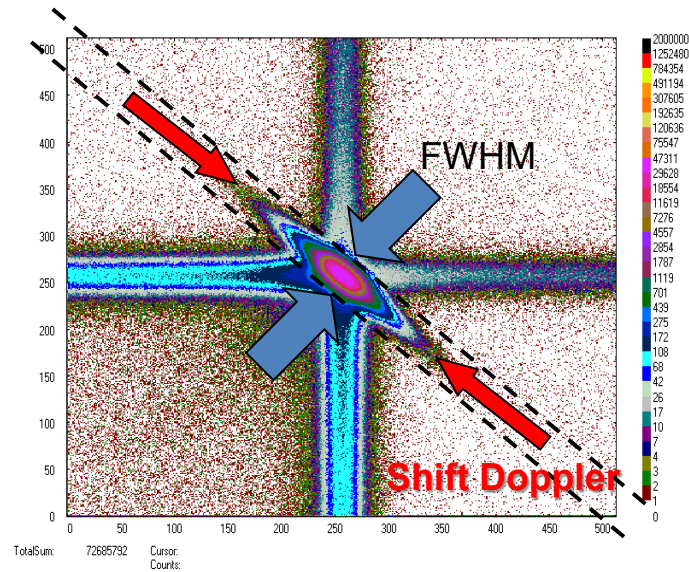
Coincidence Doppler Broadening of the annihilation radiation

Coincidence Doppler Broadening Spectroscopy (CDB)
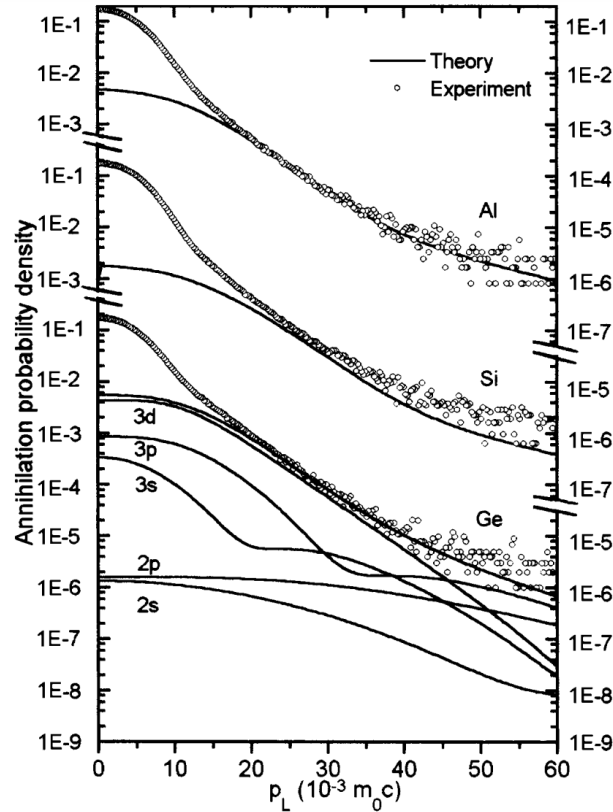
FIG. 3. The comparison of the experimental and theoretical annihilation probability densities for Al, Si, and Ge. The area under the experimental data is normalized to unity. The calculated curves have been normalized to the quantity λ_c/λ_{tot}, where λ_c and λ_{tot} are the annihilation rate with core electrons and the total annihilation rate, respectively.

Increased Elemental Specificity of Positron Annihilation Spectra

P. Asoka-Kumar,[1] M. Alatalo,[1] V. J. Ghosh,[1] A. C. Kruseman,[2] B. Nielsen,[1] and K. G. Lynn[1]
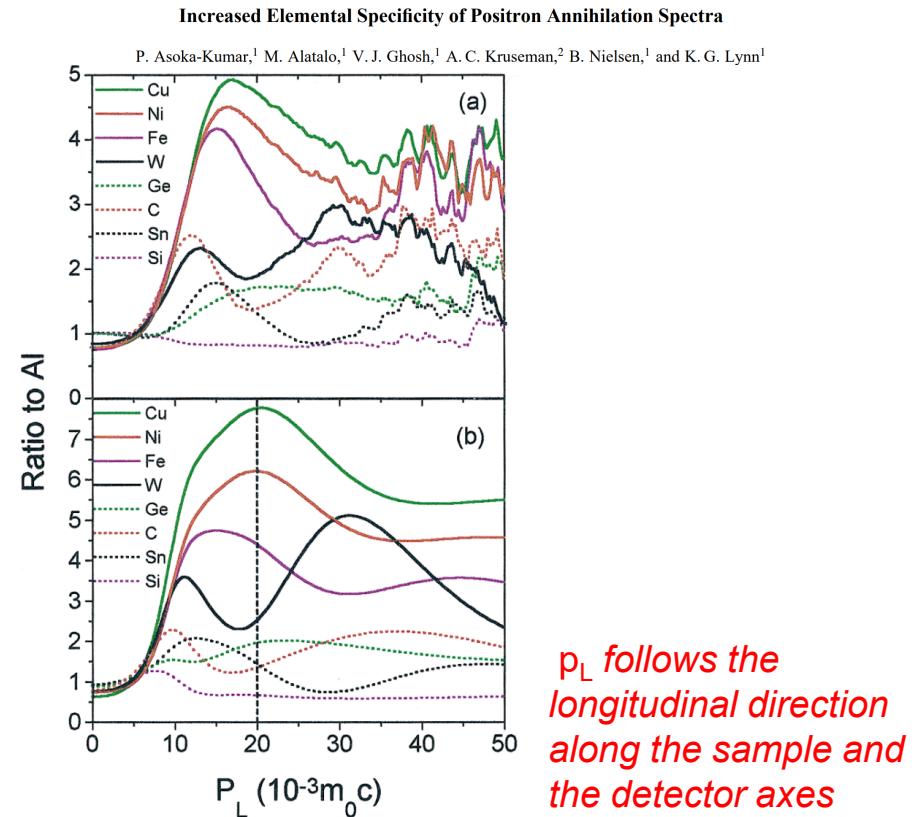
FIG. 4(color). The spectrum for different elements after normalizing to Al: (a) experiment and (b) theory. The theoretical curves for $p_L < 20 \times 10^{-3} m_0 c$ [dashed line in (b)] are not accurate.

p_L follows the longitudinal direction along the sample and the detector axes

Coincidence Doppler Broadening Spectroscopy (CDB)
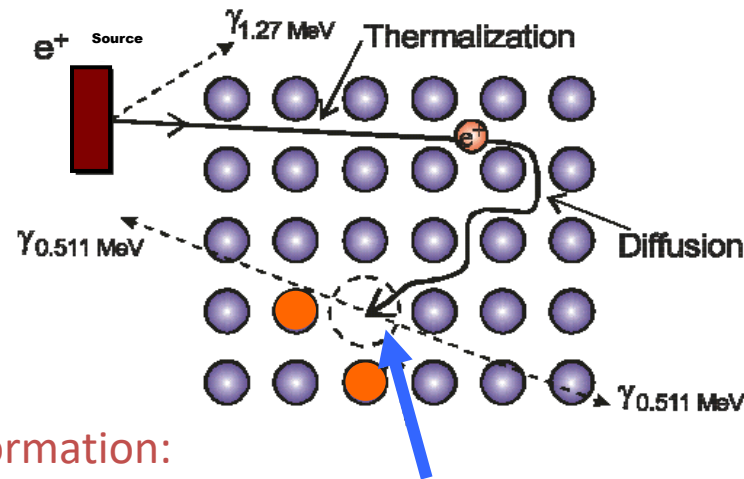

Information:

PALS: Defect concentration (trapping fraction)

CDB: Chemical environment of defects

CDB results

○ G. Pagot, V. Di Noto, K. Vezzu`, B. Barbiellini, V. Toso, A. Caruso, M. Zheng, X. Li, R. Ferragut. *Quantum view of Li-ion high mobility at carbon-coated cathode interfaces*. iScience 26, 105794 (2023).

Momentum distribution:

$$N(p_L) = -\kappa \, p_L \frac{dI(p_L)}{dp_L}$$

CDB results
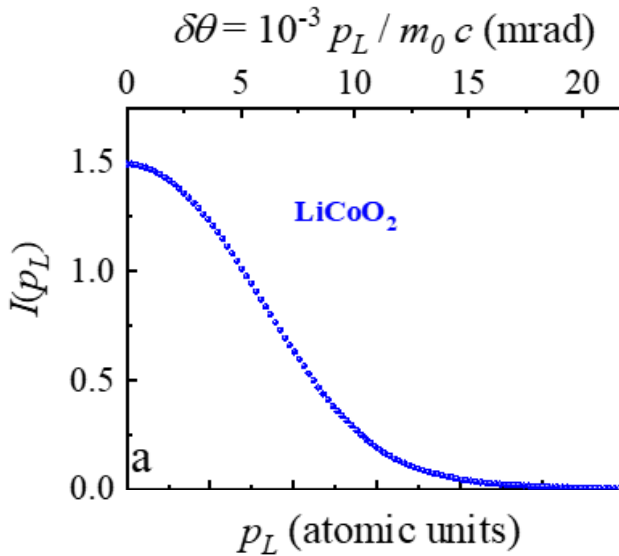
Exampl e

$I(p_L)$

p_L
(mrad)

Stewart, A.T. (1957). Momentum Distribution of Metallic Electrons by Positron Annihilation. Canadian Journal of Physics *35*, 168-183. 10.1139/p57-020.

MOMENTUM IN UNITS OF 2 mc X 10³

ENERGY — ONE PARTICLE MOVING

Momentum distribution:

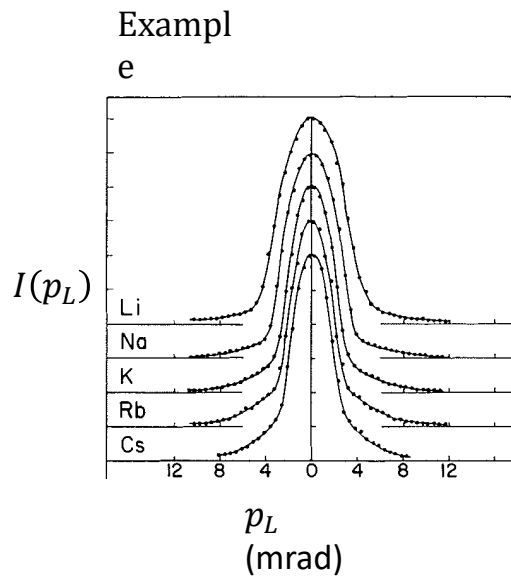$$N(p_L) = -\kappa \, p_L \, \frac{dI(p_L)}{dp_L}$$

CDB results

○ G. Pagot, V. Di Noto, K. Vezzu`, B. Barbiellini, V. Toso, A. Caruso, M. Zheng, X. Li, R. Ferragut. *Quantum view of Li-ion high mobility at carbon-coated cathode interfaces*. iScience 26, 105794 (2023).
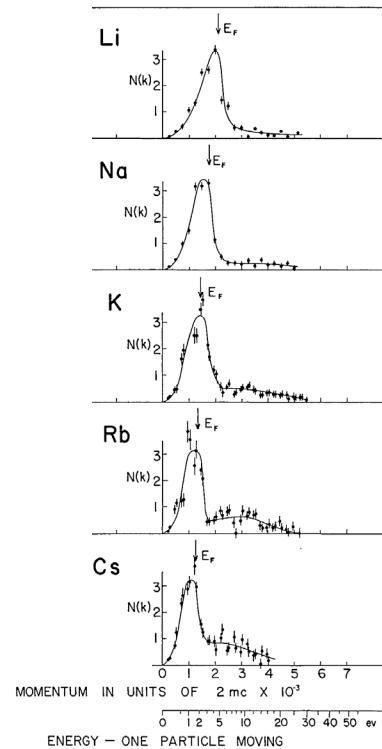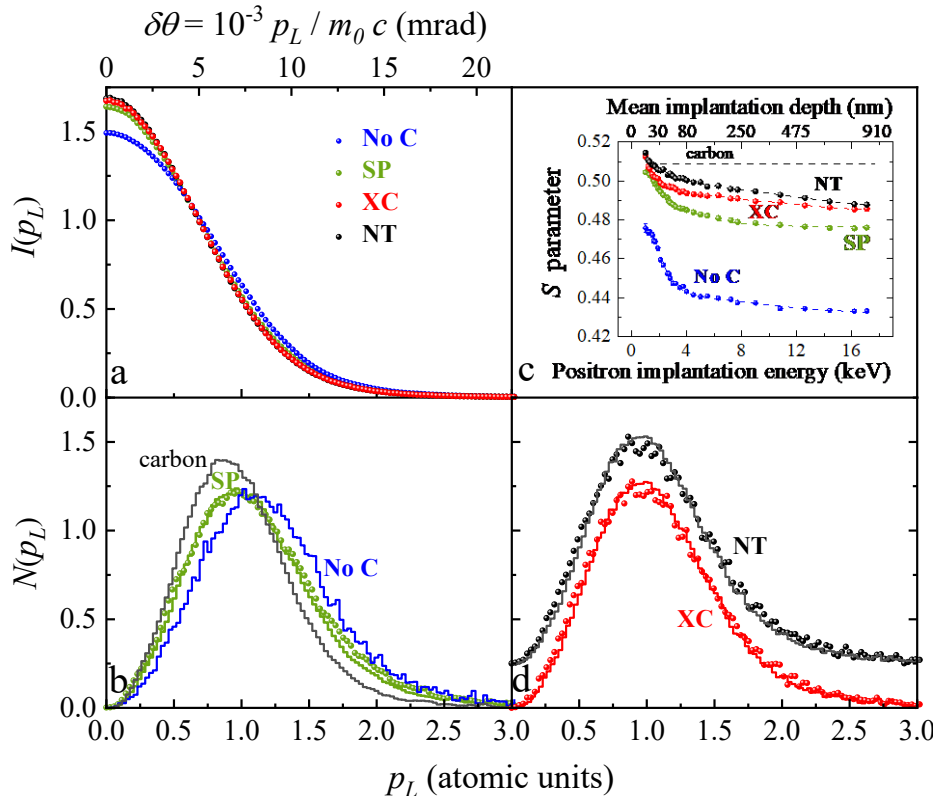
Momentum distribution:

$$N(p_L) = -\kappa \, p_L \frac{dI(p_L)}{dp_L}$$

Linear combination:

$$N(p_L) = (\beta - 1) \cdot N_{LCO_{No\,C}}(p_L) + \beta \cdot N_C(p_L)$$

The average lifetime $\bar{\tau}_E$ can be estimated by

$$\lambda_E = \bar{\tau}_E^{-1} \cong (1 - \beta) \cdot \tau_1^{-1} + \beta \cdot \tau_2^{-1}$$

Results of the linear combination proposed to test the consistency of the lifetime and CDB measurements. $\bar{\tau}_m$ is the measured value.

Coincidence Doppler broadening of the annihilation radiation of the studied cathode materials. (a) Distribution of the annihilation peak intensity $I(p_L)$ (normalized in area). (b, d) Momentum distribution $N(p_L)$ associated to the high momentum electron contribution. *NT* distribution is translated adding $0.25 \, N(p_L)$. (c) S parameter evolution as a function of the positron implantation energy.

Cathode	β	$\bar{\tau}_E$(ps)	$\bar{\tau}_m$(ps)
SP (Super P)	0.45 (3)	201 (4)	197 (3)
XC (nanospheres)	0.55 (4)	232 (5)	231 (4)
NT (nanotubes)	0.60 (3)	235 (4)	233 (3)

CDB simulations
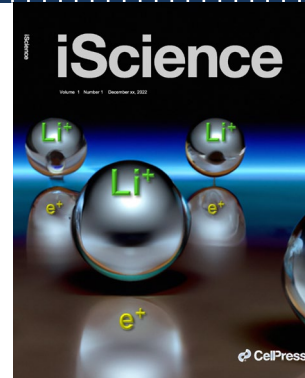
Momentum distributions
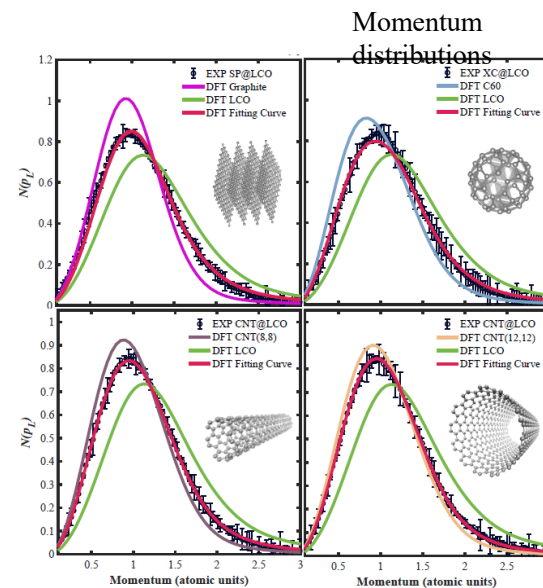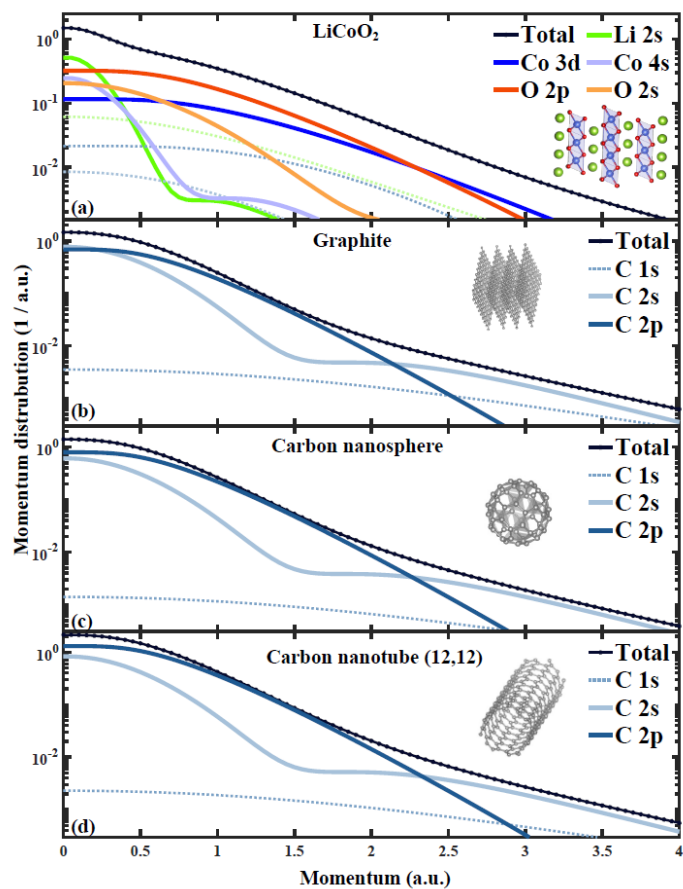
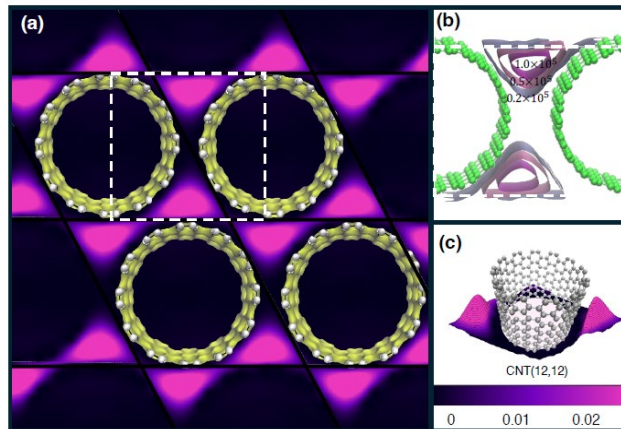Computed Doppler spectra for (a) LiCoO$_2$. (b), (c) and (d) show the graphite, nanosphere (C60), nanotube (CNT-12), respectively. Valence orbitals are shown in solid lines, and contributions from core electrons are indicated with dashed lines.

Positron localization

(a) The positron density of CNT-12 is mapped, with areas of high density depicted in purplish-red and the electron density of the carbon nanotubes shown in yellow. (b) Within the white dashed square in (a), the positron potential energy is shown in green, and the positron wavefunctions between the nanotubes are marked on isosurfaces. (c) A three-dimensional mapping of the positron density on the 001 plane.

CDB simulations

Momentum distributions
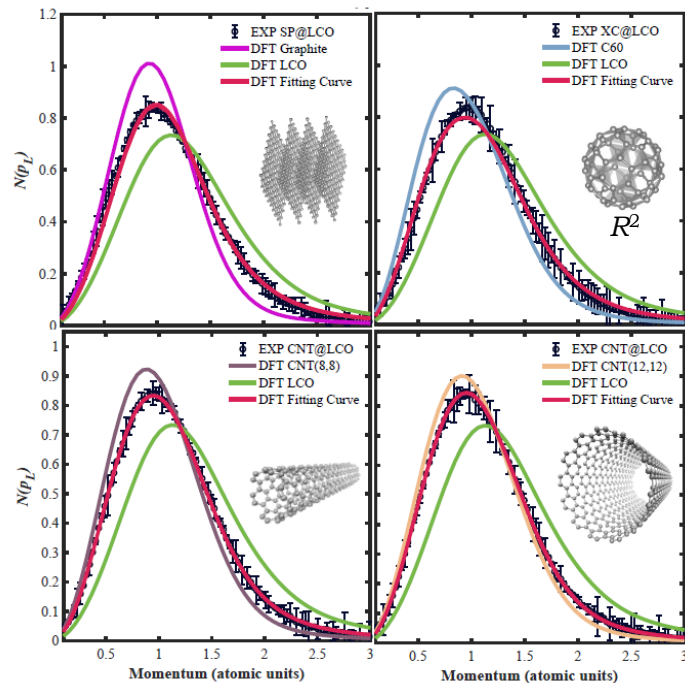
Linear Combination of DFT and EXP

		a^*	β^*	Adjusted R^2
SP	Graphite	0.496	0.504	99.731%
XC	C60	0.426	0.574	99.656%
NT	CNT-8	0.344	0.656	99.966%
CNT-12		0.250	0.750	99.983%

Momentum distributions, N (P_L) for calculates LCO and carbon, along with their linear combination, compared with experimental results from diverse samples. The momentum profiles for different measured sample types in (a) SP, (b) XC, and (c-d) NT, are represented by black symbols. The linear combination of the calculated spectra is denoted by the red solid line.
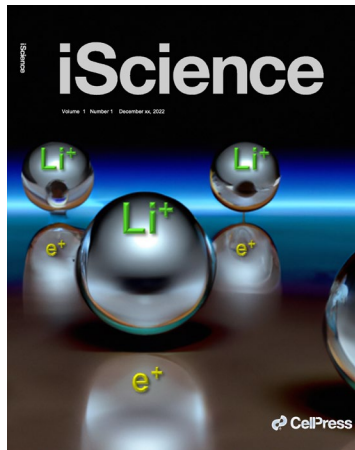
Positrons as a quantum probe

iScience

Quantum view of Li-ion high mobility at carbon coated cathode interfaces

Gioele Pagot,[1,6,*] Vito Di Noto,[1,6,**] Keti Vezzù,[1] Bernardo Barbiellini,[2,3] Valerio Toso,[4,5] Alberto Caruso,[4] Meiying Zheng,[2,4] Xin Li,[2,4] and Rafael Ferragut [3,4,6,***]